...When someone asks about applications in my talks, I usually tell a story about how I was on a boat one day watching dolphins, and they were jumping out of the water, allowing people to nearly touch them. Everyone was mesmerized by these magnificent creatures. It was an extraordinary romantic moment – well, until a little boy shouted out, "Mom, can we eat them?" It's a similar matter here – as in, okay, we just found this extraordinary material, so we're enjoying this romantic moment, and now people are asking if we can eat it or not. Probably we can, but you have to step back and enjoy the moment first.

A. Geim (Nobel Prize in Physics, 2010)

University of Alberta

Midgap states in gapped graphene induced by short-range impurities

by

Stepan Grinek

A thesis submitted to the Faculty of Graduate Studies and Research
in partial fulfillment of the requirements for the degree of

Master of Science
in
Micro-Electro-Mechanical Systems and Nanosystems

Department of Electrical and Computing Engineering

Spring 2011
Edmonton, Alberta

Examining Committee

Dr. Jie Chen, Electrical and Computing Engineering (supervisor)

Dr. Michael Brett, Electrical and Computing Engineering

Dr. Hao Zhang, Chemical and Materials Engineering

To

My Mother

Abstract

Graphene is a recently created truly two-dimensional carbon material with promising properties. It is a prospective candidate for the next generation of microelectronics. Current carriers in graphene have relativistic properties, its lattice is very strong and yet flexible, granting graphene's ballistic conductivity on the submicron scale at the room temperatures.

Midgap bound state induced by a single impurity in graphene does not cause essential changes in the electronic liquid distribution at all reasonable values of the coupling strength. Thus there are no unusual screening effects predicted for the graphene with long-range Coulomb impurity. This result holds in case of multiple impurities localized in the finite area on the lattice. Exact expressions for the lattice Green functions are derived.

The absence of critical screening for the short-range impurities in graphene is a main result of the work. Another outcome is the observation of the limitations on the Dirac approximation applicability.

Preface

Graphene is a two dimensional allotrope of carbon (2). In this thesis electronic properties of gapped graphene are discussed, i.e the properties of graphene modified in a such way that there is a non-zero gap in the energy spectrum between the valence and conductance band. Presence of this gap might be critical for the industrial applications of newly discovered material. Graphene is already attracted lots of attention from both scientific and industrial communities as a prospective substitute for the silicon in computer microchips. Its physical properties are very unusual and due to this fact graphene is often called in literature "playground" for two-dimensional Quantum Physics, especially Quantum Electrodynamics and Particle Physics.

Electronic structure of graphene was investigated a for long time. Back in 1947 ([2]), it was pointed out that electrons in honeycomb lattice have the relativistic properties. The term "graphene" was introduced in 1994 [4]. Before graphene's successful synthesis in 2004, it was believed that 2D crystals can not exist in the suspended state because of heat fluctuations, as it was stated by the theoretical works by L. Landau and R. Peierles. Discovery of graphene by A. Geim and K. Novoselov, proved that 2D crystals can be created in a suspended state and will not collapse in nanotubes or any 3D-structures (1). The reason is that naturally ever-present corrugations prevent heat excitations from destroying the crystal. Since the discovery of graphene there was constantly growing interest to this new material. It has fascinating physical properties. Graphene is an exceptional electric current conductor, with the bulk conductivity of the order of conductivity of copper, and its thermal conductivity is about 10 times better than that of copper. Graphene

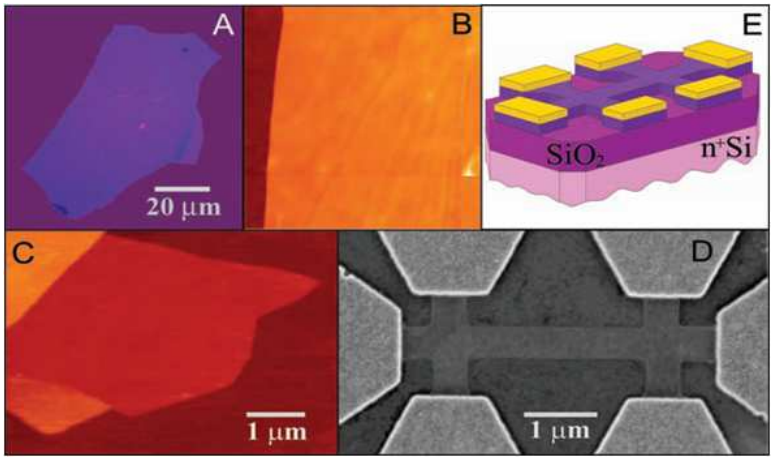

Figure 1: Image from [1], on insets **a,b,c** — samples of graphene visualized by atomic force microscope, **d,e** - first field effect transistor on graphene crystal.

exhibits properties of the quantum 2D systems even at room temperatures, as it was demonstrated K. Novoselov *et al* in their Quantum Hall Effect experiments [1] . This effect makes graphene a suitable material to built a high precision resistance standard. Graphene is also flexible and very strong material and as such is a prospective material for an electronic equipment designated to work under intense mechanical stresses.

As a promising material for microelectronics, graphene has one important feature — it is a semimetal or a zero-gap semiconductor, rather than a semiconductor. Without a gap it is impossible to control conductivity in graphene in the usual manner as it is done in silicon microelectronics with the high degree of integration. There are essentially two methods of introducing the gap in otherwise gapless energy spectrum of graphene. It is known [6], that energy gap arises as a result of geometric effect, or quantum confinement of an electron in the potential well with infinite depth. Such a scenario is realized in the graphene nanoribbons, strips cut from graphene. Despite being a very natural and most obvious way to create a

gap, quantum confinement has a disadvantage - the gap width depends on the size and shape of the ribbon and affected by the edge geometry. This complicates the design of the electronic devices and limits their possible sizes. Another set of methods is based on the idea breaking the various kinds symmetries in the honeycomb lattice. Functionalization of the π-electron bonds by chemisorption of hydrogen on the graphene surface changes sp^2 hybridized graphene into sp^2 graphane. This material receives most of the attention from researchers now among all semiconducting graphene modifications. Another way to break the symmetry and make graphene a semiconductor is a modification of the energies of the constituting carbon atoms which can be achieved chemically, by the attachment to it its surface atoms or molecules or by spatial modulation of potential in the plane of the graphene sheet. Examples are epitaxial graphene, chemically modified graphene, fully hydrogenated graphene or graphane. In the article [5] authors report experiments with hydrogenation of the quasi-freestanding graphene leading to formation of the gap of the order of 1 eV, which is dependent on the ratio between numbers of carbon and hydrogen atoms. In graphane where the hydrogenation ratio is close to unity, the band is as wide as 3.5 eV.

Charge carriers in gapped graphene have interesting physical properties. Electron transport similarly to the case of gapless graphene is governed by the relativistic Dirac equation but with massive electrons. This makes graphene a showcase for Two-Dimensional Quantum Electrodynamics (2D QED). The major difference between the 2D quasi-particles in graphene and usual electrons in 3D or 2D in vacuum is the value of the fine structure constant responsible for the intensity of electromagnetic interactions. This so cold strong-field electrodynamics makes possible to model processes yet unavailable in High Energy Physics' experiments.

One can mention, as an example, the hypothetical "vacuum charging" due to the particle-antiparticle pairs creation in the strong electric fields of heavy ions. The obstacle to observe this effect in conventional QED is that the charge of the ions must be so high that there are no stable elements with such atomic numbers. In graphene, however, these effects can be observed at charges of the order of proton charge.

Another example, Klein paradox, the ability of ultra-relativistic fermions to penetrate the potential barriers without being bounced back. This effect has not been experimentally observed either. While in graphene P. Kim group [8] was able to device an experimental set up and perform experiments which are believed to be an experimental evidence of Klein scattering of the electrons.

What is important for the applications is the graphene electronic properties in the presence of impurities and other defects, such as functional groups. Obviously, defects significantly modify conductivity of the material. Regulating the concentration of impurities, for example, one can observe the metal-insulator transition. Among the experimentally confirmed defects in graphene one can mention vacancies and noble gases ion impurities [9]. Important functional groups are carbon-based groups, hydrogen, oxygen, fluorine [10], as they turn graphene into an insulator. Fluorine, for example, has 3 eV energy gap between conductance and valence bands.

Understanding how impurities and defects modify the electronic structure near the Fermi level is critical for understanding the scattering of the conductance electrons and thus crucial for transport properties [12]. Pereira *et al.* [11] have shown that long—range Coulomb potential, confines the electronic density at the top of the valence band in a small bump several inter-atomic distances wide, and

this local negative induced charge screens the Coulomb potential in such a way that the observed potential of the Coulomb impurities is rendered as effectively a short-range one.

In our present theoretical work we consider the gapped graphene and specifically a short-range potential inducing an midgap bound states in it. Potential can be imposed by some special set up of external electric field or impurities and functional groups attached to the surface of the material. Those functional groups or impurities change energy on-site, and sufficiently large numbers of those can effectively mimic a potential in which the electrons move. Here one of the important questions arise: to what extent long-wave Dirac approximation is sufficient to describe scattering processes in the short-range potential? Thus, we consider those processes from two points of view. The first one is tight-binding approximation on the lattice, and second one is the Dirac approximation in the case of circular potential which models short-range potential on the lattice. The comparison of results derived using those two approaches shows that while it is sufficient to define the long-range behavior of the wave functions at the energies around the Dirac point, essential details of the energy level structure are better seen from the tight binding computations.

The first chapter contains the descriptions of methods used in our research. In the second chapter we present the results obtained in the thesis. A summary of the results derived and their status in the context of current research in the field are outlined in the Conclusion. The results presented in this thesis were obtained during the course of the author's MSc. program at the University of Alberta under the supervision of Prof. J. Chen in the collaboration with Prof F. Marsiglio, Zhou Li. The results are published in the paper "Absence of Supercritical Behavior in

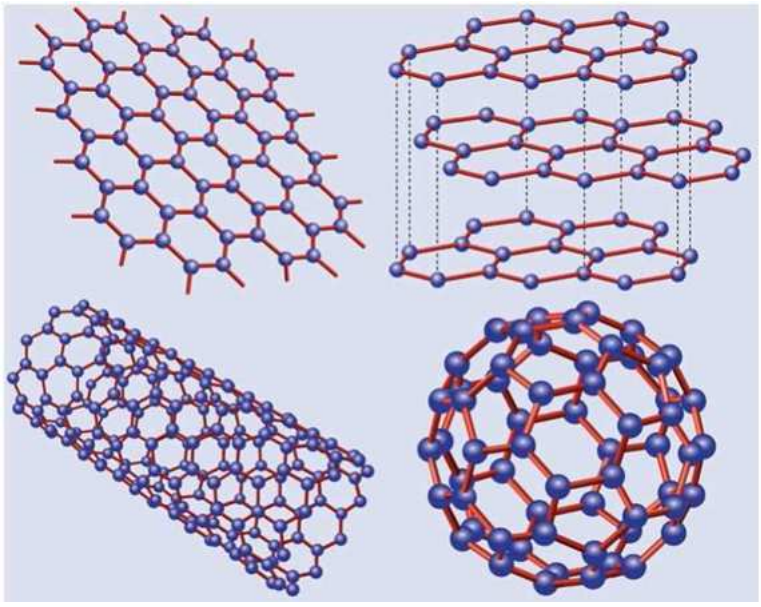

Figure 2: Graphene allotropes [7], clockwise: graphene, graphite, fullerene, nanotube

Gapped Graphene with Short-range Impurity Scattering", submitted to "Physical Review B". and presented at the conference "APS March Meeting 2010" in Portland, US.

Acknowledgements

I am happy to acknowledge the invaluable help by all the people I was lucky to work and communicate with while being a student at the Electrical and Computing Engineering Department at the University of Alberta. First, I would like to thank my scientific supervisor Prof. Jie Chen for all the time and attention he gave to me. I would also like to thank Prof. Frank Marsiglio who become de-facto my second supervisor and his student and my colleague Zhou Li, whose intelligence and computer skills made this work possible. I will always be grateful to my co-workers and friends Illia Utkin and Aleksander Lytkin for numerous discussions we had at the lounge on the third floor in ECERF. Appreciate help and enormous support I received from my friend Victor Leontyev from NINT.

Important to me is my connection with professors, students and researchers at Physical Department of University of Alberta, I want thank: Shohreh Abdolrahimi, Massimo Boninsegni, Patrick Connell, Long Dinh Dang, Dan Gorbonos, Rituparno Goswami, Faqir Khanna, David Kubizňák, Ian Mann, Allison Solanki, Eric Woolgar, Michael Woodside, Andrei Zel'nikov.

Finally, I would like to thank Kathleen Forbes, Erin Lee for their numerous help and support. My special thanks to Pinder Bains and Sandra Peake-Thibodeau for their kindness, constant help, and advices during my MSc program.

Table of Contents

List of Figures

List of Symbols and Abbreviations

This is a list of the most frequently used notations. Notations which are not explained here are explained in the text.

Abbreviations

The capital D is used for 'dimensional',i.e, 3D means 3-dimensional. QED stands for Quantum Electrodynamics, eV is an electronvolt. DOS — density of states, LDOS — local density of states.

Units

The following units convention is used in this thesis: $c = \hbar = k_B = 1$. In Chapters 1 and 2, we take $G = 1$, and in Chapter 3 we take, for convenience, $16\pi G = 1$. Here, the fundamental constants are:

the speed of light in vacuum:	$c = 299792458\ m\,s^{-1}$
the reduced Planck constant:	$\hbar = 1.054571628(53) \times 10^{-34}\ kg\,m^2\,s^{-1}$
the Boltzmann constant:	$k_B = 1.3806504(24) \times 10^{-23}\ kg\,m^2\,s^{-2}K^{-1}$

Symbols and sign conventions

The signature of the spacetime metric $g_{\alpha\beta}$ is: $(-\ +\ +\cdots+)$, i.e., it is $+(D-2)$.
The time coordinate index is 0: $t \equiv x^0$.
Balance of indices and the Einstein summation convention are assumed.

The following special symbols are used:

$\sim$	order of magnitude estimate
$\approx$	approximately equal
$\equiv$	identity
$i = \sqrt{-1}$	imaginary unit, if it sits on the baseline
$a \to b$	a goes to b
$f\|_{x=a}$	value of $f = f(x)$ evaluated at $x = a$
$\|a\|$	absolute value of a
$\mathrm{Re}(a)$	real part of a
$\mathrm{Im}(a)$	imaginary part of a
$\delta(x)$	the Dirac delta function
$\theta(x) = \begin{cases} 1, & x > 0 \\ 0, & x < 0 \end{cases}$	the Heaviside step function

The Kronecker symbol $\delta_{\alpha,\beta}$ is

$$\delta_{\alpha,\beta} = \begin{cases} 1, & \text{if } \alpha = \beta \\ 0, & \text{otherwise.} \end{cases}$$

Chapter 1

Theoretical methods

This chapter contains short description of analytical methods our research group used.

1.1 Tight-binding approximation

This section describes the most important method we applied to our object of study. Tight binding approximation is a very popular model for studying the electronic band structure of crystals. The method reduces the problem of electron motion in the periodic potential to a matrix problem defined by the limited number, usually below ten, of scalar parameters. Despite its simplicity, the tight-binding approximation is known to give correct predictions for the electronic structures of various dielectrics and semiconductors. It is well known that for the electrons in periodic potential only exactly solvable model is one-dimensional Kronig – Penney model with a sequence of rectangular potential barriers and thus, numeric methods to derive the band structure of the materials are very useful. The tight-binding

model allows analytical derivation of electronic spectra. It is also convenient for numerical computations, as it reduces Schrodinger equation to the eigenvalue problem with sparse matrix.

The discussion of this section is mainly based on books [14] and [13]. The assumptions made to derive the tight-binding model are:

1. Electrons are tightly bound to the atoms composing the crystal lattice. As a result, a linear combination of isolated atomic orbitals should be a good approximation to the single electron wave function.

2. Number of neighbors for each atom should not be too big.

3. Bands of single electronic states are not too wide.

These requirements are interrelated and the meaning of each of them will become clear from the rest of this section.

The description of tight-binding model in terms of Hamilton operator is as follows. Let H_0 be a sum of Hamilton operators H_a of the single atoms, located in the nodes of the lattice:

$$H_0(\mathbf{r}) = \sum_{\mathbf{r}_n} H_a(\mathbf{r} - \mathbf{r}_n), \tag{1.1}$$

where $\mathbf{r_n}$ are the nodes of the crystal. We ignore spin everywhere, as we do not consider the effects of magnetic fields in our work. The full Hamiltonian H must differ from H_0 by not very big periodic potential U: $H = H_0 + U$. For simplicity let us consider atoms with only one orbital per atom, then wave function can be written as:

$$\Psi(\mathbf{r}) = \sum_{\mathbf{r}_n} a(\mathbf{r}_n)\phi(\mathbf{r} - \mathbf{r}_n), \tag{1.2}$$

where $\phi(r)$ is a wave function of an electron on the isolated atom, $a(\mathbf{r}_n)$ is an

"envelop" function, introducing the influence of atoms on each other inside the lattice. We need to solve (with certain approximation) the Schrodinger equation:

$$H\Psi = E_k\Psi, \tag{1.3}$$

E_k is a Bloch energy of single electron, $\mathbf{k}$ is a Bloch momentum of electron. Here and everywhere else in this section the index k on the wave function is omitted. Bloch theorem states that the wave function in the periodic potential must satisfy the condition $\Psi(\mathbf{r}+\mathbf{r}_n) = \exp(i\mathbf{k}\mathbf{r}_n)\Psi(\mathbf{r})$, which after substitution into (1.2) gives

$$a(\mathbf{r}_n) = \exp(i\mathbf{k}\mathbf{r}_n)a(0). \tag{1.4}$$

Now we multiply left and right sides of (1.3) by the single atomic wave function and integrate over the lattice:

$$E\int \phi^*\Psi d\mathbf{r} + \int \phi^* U(\mathbf{r})\Psi d\mathbf{r} = E_k \int \phi^*\Psi d\mathbf{r} \tag{1.5}$$

$$(E_k - E)\int \phi^*\Psi d\mathbf{r} = \int \phi^* U(\mathbf{r})\Psi d\mathbf{r}, \tag{1.6}$$

where E is the energy. From (1.2 and 1.4) we obtain:

$$\Psi(\mathbf{r}) = \sum_{\mathbf{r}_n} \exp(i\mathbf{k}\mathbf{r}_n)a(0)\phi(\mathbf{r}-\mathbf{r}_n) = a(0)\sum_{\mathbf{r}_n} \exp(i\mathbf{k}\mathbf{r}_n)\phi(\mathbf{r}-\mathbf{r}_n), \tag{1.7}$$

and substituting this into (1.5) gives:

$$(E_k - E)\int \phi^* \sum_{\mathbf{r}_n} \exp(i\mathbf{k}\mathbf{r}_n)\phi(\mathbf{r}-\mathbf{r}_n)d\mathbf{r} = \tag{1.8}$$

$$= \int \phi^* U(\mathbf{r}) \sum_{\mathbf{r}_n} \exp(i\mathbf{k}\mathbf{r}_n)\phi(\mathbf{r}-\mathbf{r}_n)d\mathbf{r}. \tag{1.9}$$

This is a secular equation we wanted to obtain. However, left in this state it is not very useful for numerical or analytical computations as it contains infinite sums of integrals. To simplify it further we neglect all terms with atomic wave functions which are not centered on the same node or at next closest atoms. This is called "next-neighbor approximation":

$$(E_k - E)(\sum_{n.n.} \alpha(\mathbf{R})\exp(i\mathbf{k}\mathbf{R}) + 1) = \sum_{n.n.} \gamma(\mathbf{R})\exp(i\mathbf{k}\mathbf{R}) + \beta, \tag{1.10}$$

we also made an assumption that the potential U is circularly symmetric. The notations introduced are:

$$\alpha(\mathbf{R}) = \int \phi^*(\mathbf{r})\phi(\mathbf{r}-\mathbf{R})d\mathbf{r} \tag{1.11}$$

$$\beta = -\int \phi^*(\mathbf{r})U(\mathbf{r})\phi(\mathbf{r})d\mathbf{r} \tag{1.12}$$

$$\gamma(\mathbf{R}) = -\int \phi^*(\mathbf{r})U(\mathbf{r})\phi(\mathbf{r}-\mathbf{R})d\mathbf{r}, \tag{1.13}$$

n.n. stands for "next closest neighbor" and we arrive to the dispersion expression:

$$E_k = E + \frac{\beta + \sum_{n.n.}\gamma(\mathbf{R})}{1 - \sum_{n.n.}\alpha(\mathbf{R})\exp(i\mathbf{k}\mathbf{R})} \tag{1.14}$$

Now we can comment on the meaning of the Greek coefficients. The coefficient α should be small as it is an overlap integral between single atomic functions. The magnitude of γ determines the band width. This overlap integral is small by the assumption potential U and henceforth tight-binding bands should be narrow, β is a shift of the isolated atomic energy level caused by the potential U.

1.2 Dispersion law and Dirac formalism derivation

Suspended graphene has quasi-relativistic electronic spectrum, an attribute of zero-mass fermions. As it will be shown below the electrons remain relativistic even upon the introduction of the gap. Quasi-particles become similar to relativistic massive electrons confined in 2D. In this section we give a simplified introduction into pseudo-relativistic physics in honeycomb lattice with a gap.

We use tight-binding model introduced in the pervious section. This time, though, reasoning is different as graphene has two sublattices (1.1), A and B or, in the other words, its unit cell is diatomic. Thus we write the wave function as a sum [2]:

$$\Psi(\mathbf{r})_A = \sum_{\mathbf{r}_A} \exp(i\mathbf{k}\mathbf{r}_A)\phi(\mathbf{r}-\mathbf{r}_A), \tag{1.15}$$

$$\Psi(\mathbf{r})_B = \sum_{\mathbf{r}_B} \exp(i\mathbf{k}\mathbf{r}_B)\phi(\mathbf{r}-\mathbf{r}_B), \tag{1.16}$$

here $\Psi(\mathbf{r})_A$ and $\Psi(\mathbf{r})_B$ are the electron wave function on the sublattices A and B

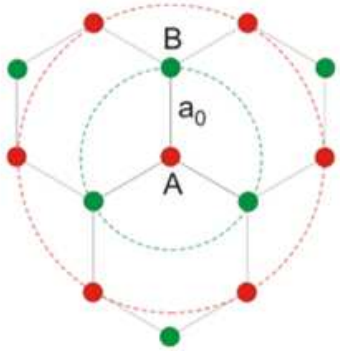

Figure 1.1: Two sublattices in graphene. Inner circle includes "closest neighbors" atoms.

correspondingly. The full wave function is

$$\Psi(\mathbf{r}) = \Psi(\mathbf{r})_A + \lambda\Psi(\mathbf{r})_B, \tag{1.17}$$

λ is a constant parameter to be eliminated later. The Hamiltonian of the system is the one that was defined in previous section with addition of periodic M-operator:

$$H_0(\mathbf{r}_C) = H_0 + U + M(\mathbf{r}_C), \tag{1.18}$$

the M-operator is defined as follows:

$$M(\mathbf{r}_C) = \begin{cases} +m & \text{if } C = A \\ -m & \text{if } C = B. \end{cases} \tag{1.19}$$

This operator introduces effect of the underlying lattice or external periodic field opening the gap with the width of $2m$. After multiplication of the Hamiltonian operator (1.18) by the atomic wave function ϕ_A, centered at one of the A-sites from the left side and by the full wave function Ψ from the right side we obtain:

$$E_k - E - m = \lambda \sum_{n.n.} \gamma(\mathbf{R}_B) \exp(i\mathbf{k}\mathbf{R}_B) + \beta, \tag{1.20}$$

we assumed that overlap between the neighboring atomic functions is negligible, i.e $\alpha(\mathbf{r}_C) = 0$. Let us repeat this procedure with an atomic orbital ϕ_B, centered at the one of the sites on B-sublattice:

$$\lambda(E_k - E - m) = \sum_{n.n.} \gamma(\mathbf{R}_B) \exp(i\mathbf{k}\mathbf{R}_B) + \lambda\beta, \tag{1.21}$$

Due to the symmetry of the lattice $\gamma(\mathbf{R}_C) = \gamma(|\mathbf{R}_C|)$. We kept in the sums only $\mathbf{R}_C$ which connects the nearest neighbors, hence the notation "$n.n.$". We arrive to the system of equations:

$$E_k - E - m = \lambda\gamma S_B + \beta \tag{1.22}$$

$$\lambda(E_k - E - m) = \gamma S_A + \lambda\beta, \tag{1.23}$$

where γ is the value of $\gamma(\mathbf{R}_C)$ at the next closest neighbour,

$$S_A = e^{iak_y} + e^{ia(-k_x\sqrt{3}/2 - k_y/2)} + e^{ia(k_x\sqrt{3}/2 - k_y/2)}, \tag{1.24}$$

$$S_B = e^{-iak_y} + e^{ia(-k_x\sqrt{3}/2 + k_y/2)} + e^{ia(k_x\sqrt{3}/2 + k_y/2)}, \tag{1.25}$$

a is a lattice constant. Solving system (1.22) we get the dispersion law with a gap

of $2m$ centered at the energy β: $E_k = \beta \pm \sqrt{\gamma^2 S_B S_A + m^2}$. One can shift the energy spectrum, so that center of the gap is at the zero energy:

$$E_k = \pm\sqrt{\gamma^2 S_B S_A + m^2}. \tag{1.26}$$

In what follows we choose $a \equiv 1$ to keep notation simple and restore the dimensionality where it is necessary. Performing straightforward algebraic and trigonometric simplification we obtain:

$$E_k = \pm\sqrt{\gamma^2(1 + 4\cos^2\sqrt{3}k_y/2 + 4\cos 3/2k_x \cos\sqrt{3/2}k_y) + m^2}. \tag{1.27}$$

Tight-binding approximation introduced in the previous section can be represented in the single-particle formalism of creation and annihilation operators. Starting with Bloch states $|\psi_{\mathbf{k}}>_{A,B}$ one can define basis functions called Wannier states $|\psi_{\mathbf{R}}>_{A,B}$ as:

$$|\psi_{\mathbf{R}}>_A \equiv \frac{1}{\sqrt{N}}\sum_{\mathbf{k}} \exp(-i\mathbf{k}\mathbf{R}_A)|\psi_{\mathbf{k}}>_A, \tag{1.28}$$

$$|\psi_{\mathbf{R}}>_B \equiv \frac{1}{\sqrt{N}}\sum_{\mathbf{k}} \exp(-i\mathbf{k}\mathbf{R}_B)|\psi_{\mathbf{k}}>_B, \tag{1.29}$$

$$|\psi_{\mathbf{k}}>_A \equiv \frac{1}{\sqrt{N}}\sum_{\mathbf{R}_A} \exp(i\mathbf{k}\mathbf{R}_A)|\psi_{\mathbf{R}}>_A, \tag{1.30}$$

$$|\psi_{\mathbf{k}}>_B \equiv \frac{1}{\sqrt{N}}\sum_{\mathbf{R}_B} \exp(i\mathbf{k}\mathbf{R}_B)|\psi_{\mathbf{R}}>_B . \tag{1.31}$$

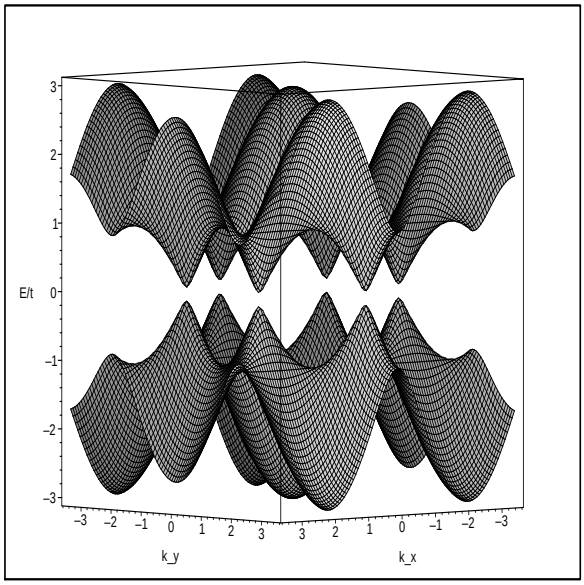

Figure 1.2: Dispersion for the gapped graphene, ratio (gap width) / t is taken to be 0.1

It is convenient to use spinor notation here, as we deal with bipartite lattice. Index A corresponds to the A-sublattice, B - to the B-sublattice, correspondingly. Thus $\{|\psi_{\mathbf{R}}>_A, |\psi_{\mathbf{R}}>_B\}$ and $\{|\psi_{\mathbf{k}}>_A, |\psi_{\mathbf{R}}>_B\}$ are bi-component spinors in real and k-space. Convenience of Wannier basis is in its orthogonality. In the limit of zero periodic potential in U these states become atomic orbitals of isolated atoms placed at the lattice sites. In this basis one can write Hamiltonian in the form:

$$H = -t\sum_{\mathbf{j},\delta}(a^{\dagger}_{\mathbf{j}}b_{\mathbf{j}+\delta} + b^{\dagger}_{\mathbf{j}+\delta}a_{\mathbf{j}}) + m\sum_{\mathbf{i}}(a^{\dagger}_{\mathbf{i}}a_{\mathbf{i}} - b^{\dagger}_{\mathbf{i}}b_{\mathbf{i}}). \tag{1.32}$$

In this representation it is usual to denote hopping parameter γ as t, δ are vectors connecting next closest sites. As usual, we introduce Fourier-transformed operators

as:

$$a(\mathbf{r_j}) = \frac{1}{\sqrt{N}} \sum_{\mathbf{k}} \exp(-i\mathbf{k}\mathbf{r_j}) a(\mathbf{k}), \tag{1.33}$$

$$b(\mathbf{r_j}) = \frac{1}{\sqrt{N}} \sum_{\mathbf{k}} \exp(-i\mathbf{k}\mathbf{r_j}) b(\mathbf{k}), \tag{1.34}$$

here $a(\mathbf{r_j}) \equiv a_\mathbf{j}, b(\mathbf{r_j}) \equiv b_\mathbf{j}$, summation is done in the first Brillouin zone. As a result of this transformation the Hamiltonian (1.32) is represented in the following form:

$$H = \sum_{\mathbf{k}} \left(a(\mathbf{k})^\dagger b(\mathbf{k})^\dagger \right) \begin{pmatrix} m & -tS_A \\ -tS_B & -m \end{pmatrix} \begin{pmatrix} a(\mathbf{k}) \\ b(\mathbf{k}) \end{pmatrix} \tag{1.35}$$

This Hamiltonian operator is diagonal in $k-$spase but not diagonal in spinor indices. Diagonalizing this matrix one can get the dispersion law (2.12). On the figures 1.2 and 1.2 one can see two sets of equivalent Fermi points at the half-filling. On the Fig. 1.2 equivalent Fermi points (called Dirac points in the literature about graphene), connected by the vectors of the reciprocal lattice, are denoted by the white and black circles. To describe physics approximately at the half-filling it is enough to make an expansion of the Hamiltonian at any two of non-equivalent points in the Brillouin zone, say K_1 and K_2 on the Fig. 1.2. Therefore, we double the number of creation and annihilation operators, which is a reasonable thing to do as the states in the k-space are doubly degenerated. Here, we introduce

following notation:

$$a_1(\mathbf{k}) = a(\mathbf{K_1} + \mathbf{k}) \tag{1.36}$$

$$a_2(\mathbf{k}) = a(\mathbf{K_2} + \mathbf{k}) \tag{1.37}$$

$$b_1(\mathbf{k}) = b(\mathbf{K_1} + \mathbf{k}) \tag{1.38}$$

$$b_2(\mathbf{k}) = b(\mathbf{K_2} + \mathbf{k}). \tag{1.39}$$

Performing expansion of the Hamiltonian and keeping terms linear in $\mathbf{k}$ we obtain:

$$H(\mathbf{k}) = \begin{pmatrix} a_1(\mathbf{k})^\dagger b_1(\mathbf{k})^\dagger a_2(\mathbf{k})^\dagger b_2(\mathbf{k})^\dagger \end{pmatrix} \begin{pmatrix} \mathbf{H_1} & \mathbf{0} \\ \mathbf{0} & \mathbf{H_2} \end{pmatrix} \begin{pmatrix} a_1(\mathbf{k}) \\ b_1(\mathbf{k}) \\ a_2(\mathbf{k}) \\ b_2(\mathbf{k}), \end{pmatrix} \tag{1.40}$$

where $\mathbf{0}$ is a two by two matrix of zeros and $\mathbf{H_{1,2}}$ are

$$\mathbf{H_{1,2}} = t \begin{pmatrix} m/t & \frac{3}{2}(ik_x \pm k_y) \\ \frac{3}{2}(-ik_x \pm k_y) & -m/t \end{pmatrix}, \tag{1.41}$$

or

$$\mathbf{H_{1,2}} = \hbar v_f(-\sigma_2 k_x \pm \sigma_1 k_y) + m\sigma_3, \tag{1.42}$$

where $v_f = 3ta/(2\hbar)$, is a Fermi speed of the electrons, σ_i are the Pauli matrices:

$$\sigma_1 = \begin{pmatrix} 0 & 1 \\ 1 & 0 \end{pmatrix} \quad \sigma_2 = \begin{pmatrix} 0 & -i \\ i & 0 \end{pmatrix} \quad \sigma_3 = \begin{pmatrix} 1 & 0 \\ 0 & 1 \end{pmatrix}. \tag{1.43}$$

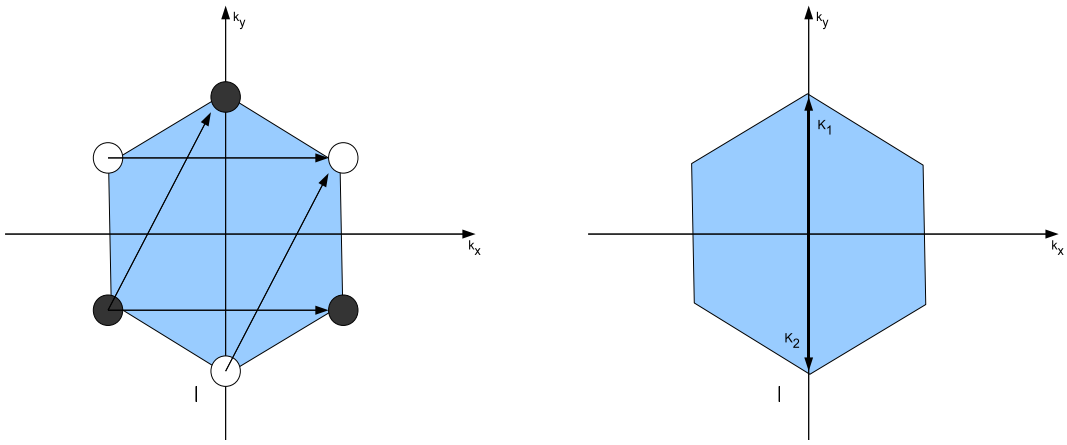

Figure 1.3: On the left picture: first Brillouin zone with equivalent points connected by reciprocal lattice vectors. On the right picture: two non-equivalent points of the Brillouin zone used for long-wave approximation described in the text, K_1 and K_2 are the two inequivalent Dirac points used to linearize Hamiltonian in their vicinity.

The next step, which is usually taken in literature, is to use bi-spinor notation [33]. We use four by four matrices:

$$\alpha_x = -\begin{pmatrix} \sigma_2 & 0 \\ 0 & \sigma_2 \end{pmatrix} \quad \alpha_y = \begin{pmatrix} \sigma_1 & 0 \\ 0 & -\sigma_1 \end{pmatrix} \quad \alpha_z = \begin{pmatrix} \sigma_3 & 0 \\ 0 & \sigma_3 \end{pmatrix}, \tag{1.44}$$

now the Hamiltonian can be written as:

$$H(\mathbf{k}) = \hbar v_f(\alpha_x k_x + \alpha_y k_y) + m\alpha_z, \tag{1.45}$$

and Fourier-transform back to the real space gives us long-wave approximation, which has the form of relativistic equation for an electron in two spatial dimensions (Dirac-Weyl equation):

$$H(\mathbf{x}) = -i\hbar v_f(\alpha_x \partial_x + \alpha_y \partial_y) + m\alpha_z, \tag{1.46}$$

here $v_f \simeq 1000$ km/s, which is about 3000 times lesser than speed of light in the original equations derived for the relativistic electrons in vacuum. One can prove that symmetric properties of the solutions of the equation

$$H(\mathbf{x})\Psi = E\Psi \tag{1.47}$$

allows to classify them as true bispinors. The sign of their wave function changes if the phase gains 2π increment. Henceforth, two "upper" components of the bispinor are related to the two "lower" ones by the time reversal transformation. Because of this in the Dirac approximation it is enough to solve the problem for just "upper" two-component spinor [34]. This approach is used in the present work as well. It is important to understand that similarity with relativistic equations is limited [35]:

1. The domain of applicability of this equation is limited to small values of $\|\mathbf{k}\|$ and slowly changing potentials. When steep potentials and/or high energies are involved, the Dirac approximation may fail. One of the main conclusions we made in the present research is that short range-potential on the graphene lattice can not be correctly approximated by the Dirac equation.

2. Equation (1.47) is only applicable in the static coordinate system and it is not invariant neither under Galilean nor Lorentz transformation. It is not Galilean-invariant as in case with any other effective mass approximation, even if original Schrödinger equation is Galilean invariant. Obviously, it can not be Lorentz-invariant as v_f is not equal to the speed of light present in the relativistic equations [35].

1.3 Density of States and Green functions

In this thesis we use Green functions for a single electron propagating on the graphene lattice in the tight-binding approximation. The general definition of the quantum-mechanical Green function can be written as [24]:

$$\hat{G}(E) = (E - \hat{H})^{-1}. \tag{1.48}$$

Let us present this operator in the basis of energy states $|\omega >$, inserting the unity operators in the above expression:

$$\hat{G}(E) = \sum_{i,j} |\omega_i >< \omega_i|(E - \hat{H})^{-1}|\omega_j >< \omega_j|, \tag{1.49}$$

noting that $\hat{H}|\omega_i >= \omega_i|\omega_i >$ and $< \omega_i|\omega_j >= \delta_{ij}$ this transforms into:

$$\hat{G}(E) = \sum_{i} |\omega_i > (E - \omega_i)^{-1} < \omega_i|. \tag{1.50}$$

To derive spatial density of states we project this operator on the basis of localized Wannier states:

$$G(E, \mathbf{x}, \mathbf{y}) = \sum_{i} < \mathbf{x}|\omega_i > (E - \omega_i)^{-1} < \omega_i|\mathbf{y} >= \sum_{i} \frac{\phi_i^*(\mathbf{x})\phi_i(\mathbf{y})}{E - \omega_i}, \tag{1.51}$$

here. $\phi_i(\mathbf{x}) =< \mathbf{x}|\omega_i >$ are single electron wave functions in coordinate representation. Now we notice that sum of all $\phi_i^*(\mathbf{x})\phi_i(\mathbf{x})$ with the same i can be defined as a probability density of the discrete state at the energy ω_i, $\rho(\omega_i, \mathbf{x})$. Integrating

over the energy instead of summation and using the functional identity

$$\lim_{\delta \to +0} \frac{1}{x + i\delta} = -i\pi\delta(x) + P\left(\frac{1}{x}\right) \tag{1.52}$$

we obtain the following expression which relates imaginary part of the Green function and the density of states:

$$Im(G(E, \mathbf{x}, \mathbf{x})) = Im \int \frac{\rho(\omega, \mathbf{x})}{E + i\delta - \omega} d\omega = -\pi \int \delta(E - \omega)\rho(\omega, \mathbf{x}) d\omega = -\pi\rho(E, \mathbf{x}), \tag{1.53}$$

or

$$\rho(E, \mathbf{x}) = -\frac{1}{\pi} ImG(E, \mathbf{x}, \mathbf{x}). \tag{1.54}$$

When related to the multiple impurities scattering the T-matrix formalism used in the previous section to describe scattering on two impurities in is basically a reformulation of the expression (2.23) in a way suitable for iterative computations. Here is a short description of the method.

Let us consider the following Hamiltonian (we omit hats over the operators):

$$H = H_0 + H_l \tag{1.55}$$

$$H_l = |l > V < l|, \tag{1.56}$$

here V is the on-site potential induced by external field or impurity, $|l >$ is a ket-vector for a Wannier state localized at the site with the multi-index coordinate l. We assume that the Green function for H_0, $G_0(E)$ is known. The Green function

operator is then written as [25]:

$$G(E) = (E - H_0 - H_1)^{-1}. \tag{1.57}$$

Performing straightforward linear algebra manipulations we obtain:

$$G = (E - H_0 - H_1)^{-1} = [(E - H_0)(1 - G_0 H_1)]^{-1} \tag{1.58}$$

$$= (1 - G_0 H_1)^{-1} G_0, \tag{1.59}$$

where $G_0 \equiv G_0(E)$, the first cofactor in the last expression can be expanded in series of $G_0 H_1$ (we consider H_1 as a perturbation):

$$G = G_0 + G_0 H_1 G_0 + G_0 H_1 G_0 H_1 G_0 + ..., \tag{1.60}$$

at this point one can define a T - matrix:

$$T = H_1 + H_1 G_0 H_1 + H_1 G_0 H_1 G_0 H_1 ..., \tag{1.61}$$

$$G = G_0 + G_0 T G_0 \tag{1.62}$$

in our case T is

$$T_l = |l > V < l| + |l > V < l| G_0 |l > V < l| + |l > V < l| G_0 |l > V < l| G_0 |l > V < l| ..., \tag{1.63}$$

noting that $< l|G_0|l >= G_0(l, l)$:

$$T_l = |l > V(1 + V G_0(l, l) + (V G_0(l, l))^2 + ...) < l|, \tag{1.64}$$

summing up terms in the parenthesizes we obtain compact expression for T-matrix:

$$T_l = |l > \frac{V}{1 - VG_0(l,l)} < l|. \tag{1.65}$$

This concludes derivation of the T-matrix in the single impurity case. One can start the next iteration from this point — using G as an unperturbed Green function derive the Green function G_m for the new system containing one more impurity at the site m:

$$G_m = G + GT_mG, \tag{1.66}$$

$$T_m = |m > \frac{V}{1 - VG(m,m)} < m|. \tag{1.67}$$

Chapter 2

Numerical and analytical results [1]

2.1 Formulation of the problem

Graphene can be used as an effective playground to study relativistic phenomena in super-heavy atoms with nucleus charge more than $150e$ because the critical charge for the Dirac fermions in graphene is of the order of unity.[11] Once one places an impurity with single elementary charge into pristine graphene lattice, a bound state splits from the bottom of the conductance band within the mass gap that separates the original Dirac cones.[15, 16] The increase of the coupling strength or the electrical charge on the impurity will drive the quantum state of the system to the critical point at which the midgap state joins the lower continuum. In heavy atoms this condition signifies a electrodynamic vacuum state stability breakdown. For the gapped graphene this means that the screening charge reshapes significantly in the vicinity of the Coulomb centre.[11] The amplitude of the merging bound state decays exponentially with the distance from the charge. When the charge is at

[1] *A version of this chapter has been submitted for publication.*

the supercritical value, the screening effect is rather strong, the observed effective charge is reduced by almost $4e$ due to double spin and valley degeneration.[11] The similar phenomenon occurs in atomic physics is unreachable at the modern experimental level charge of 170 elementary units.[17] On the Fig.() one can see corresponding energy diagrams from [17]. Left one shows that point-like charge as a center of the potential in the Dirac equation cannot exceed 137 elementary units; on the second one $1s$ orbital of the atom with finite size nucleus dives into the "Dirac see" at the charge $172e$. Complex of QED phenomena develops and as a result the nucleus charge becomes lesser by 2 elementary units. Very similar situation is shown on (2.1) for graphene with the difference that critical charge is of the order of unity instead of 172. Important for the current research in graphene is the fact that the shape of the cloud of screening charge is very close to the shape of the "critical state" on the verge of diving from the gap into the band of continuous levels. In this chapter we will try to answer two questions important for the physics of critical phenomena in graphene: i)How does the range of the potential affect the electronic structure in the part of the valence band closest to its upper edge? This is an interesting problem, as the energy levels closest to the gap control the screening properties of the electronic liquid. ii) How strong should be the potential to create critical state on graphene lattice? There is already a significant number of research papers on this subject. These problems have attracted significant research attention and the gapless graphene case has already been exhaustively studied [18]. In particular, several articles were published on exploring the properties of the midgap states. In Ref. [20], the authors studied the midgap states induced by vacancies in the long wave limit. In Ref. [21], authors considered mostly the Coulomb potential case in the Dirac approximation, and presented the

solutions of the midgap states in the presence of short-range impurities. In the presented work, we deal with the midgap states that are about to merge into the continuum both in the Dirac approximation and on a lattice where the approximation of a linear dispersion is not assumed. Unexpected at the beginning of the work, it was found that the Dirac approximation alone gives different prediction about impurity strength required for the energy level inside the gap to dive into the continuum.

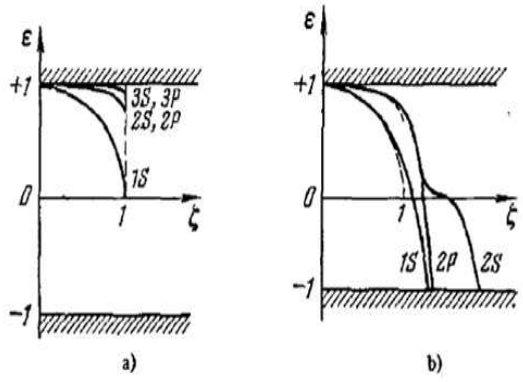

FIG. 1. The energies of the lower levels with angular momentum j = 1/2 (ζ = Z/137): a) for a point-charge potential V(r) = −Ze²/r; b) with allowance for the finite dimensions of the nucleus.

Figure 2.1: Picture from the one of the pioneering articles [17](1972). Energy diagram on the left demonstrates the breakdown of the Dirac equation with the point source of Coulomb field with the charge $137e$. On the right side: in the model with finite size of the nucleus $1s$ level joins the lower continuum

The chapter is organized as follows. In the next section we obtain the predictions of the long-wavelength Dirac formalism in the case of the short range impurity potential. The third section contains short description of the Green function formalism extensively used in our study, derive general expression for the gapped graphene Green functions. In the fourth section, the results for single—

and two—impurities cases are generalized to some extent on the case with multiple impurities.

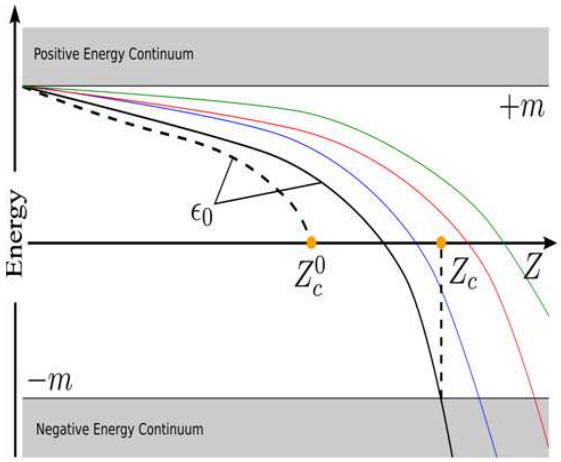

Figure 2.2: Picture from [11]. Mid-gap state joins the valence band in the field of Coulomb impurity. Results were obtained in tight-binding approximation on graphene lattice.

2.2 Dirac equation with spherical well

The equation of motion of an electron with a fixed full (pseudo-spin plus orbital) angular momentum in a circularly symmetric potential $U(r)$ is described by the spinor equations

$$\begin{aligned}(E-U(r)-m)A(r)-(\partial_r+\frac{j}{r})B(r) &= 0,\\ (\partial_r-\frac{j}{r})A(r)+(E-U(r)+m)B(r) &= 0,\end{aligned} \tag{2.1}$$

where $U(r)=V\theta(a-r)$, where $\theta(x)$ is a Heaviside step function, a is the radius of the well, and V is negative (positive) for a well (barrier). Spinor field describing the

full wave function has a meaning of two probability densities, i.e. upper component of the spinor is a probability density on the A-sublattice, and the lower component corresponds to a probability density on the B-sublattice correspondingly [11]:

$$\Psi_C(r,\phi) = \frac{1}{\sqrt{r}} \left\{ \begin{array}{c} e^{-i(j-1/2)\phi} A(r) \\ ie^{-i(j+1/2)\phi} B(r) \end{array} \right\}. \tag{2.2}$$

Here j is an eigenvalue of full momentum $J_z = L_z + \frac{1}{2}\sigma_z$, and C can refer to either the A or B sublattice. To solve Eq. (2.1), one can express $B(r)$ in terms of $A(r)$:

$$B(r) = \frac{\frac{j}{r}A(r) - A'(r)}{E - V + m}. \tag{2.3}$$

In what follows, we consider the situation when the energy level is at either gap edge; for negative (positive) V this is the lower (upper) edge. The solutions inside the well are:

$$\begin{aligned} A(r) &= C_1\sqrt{r}\sqrt{\frac{E+m-V}{E-m-V}} J_{j-1/2}(\sqrt{(E-V)^2 - m^2}r), \\ B(r) &= C_1\sqrt{r} J_{j+1/2}(\sqrt{(E-V)^2 - m^2}r). \end{aligned} \tag{2.4}$$

The solutions outside the well are:

$$\begin{aligned} A(r) &= C_2\sqrt{r}\sqrt{\frac{E+m}{E-m}} K_{j-1/2}(\sqrt{m^2 - E^2}r), \\ B(r) &= -iC_2\sqrt{r} K_{j+1/2}(\sqrt{m^2 - E^2}r), \end{aligned} \tag{2.5}$$

where $J_\alpha(x)$ is a Bessel function of the first kind, and $K_\alpha(x)$ is a modified Bessel function of the second kind chosen to satisfy the boundary condition at infinity.

The equation for the energy levels is:

$$\frac{\sqrt{\frac{E+m-V}{E-m-V}}J_{j-1/2}(\sqrt{(E-V)^2-m^2}a)}{J_{j+1/2}(\sqrt{(E-V)^2-m^2}a)} = i\frac{\sqrt{\frac{E+m}{E-m}}K_{j-1/2}(\sqrt{m^2-E^2}a)}{K_{j+1/2}(\sqrt{m^2-E^2}a)} \quad . \tag{2.6}$$

For a solution to exist, the terms on the left-hand side and on the right-hand side must be either pure imaginary or pure real numbers. This means, that for $-m \leq E \leq 0$, and with $V < 0$, we require that $(E-V)^2 > m^2$ for a solution. We are primarily interested in negative values of V. The solution for the $j = 1/2$, for example, is:

$$V = -m - \sqrt{m^2 + b_1^2/a^2}, \tag{2.7}$$

where b_1 is the first root of the Bessel function J_0.

We are interested also in what sequence the levels will merge into the continuum, depending on their angular momentum. One can numerically analyze Eq. (2.6) but for the sake of clarity we will analyze the effective Schrodinger equation for $A(r)$, obtained from the system (2.1):

$$-A''(r) + [\frac{j^2-j}{r^2} - (E-V)^2 + m^2]A(r) = 0. \tag{2.8}$$

This is a wave equation for a particle in a potential with functional form $\frac{j^2-j}{r^2} - (E-V)^2+m^2$ at zero energy. Obviously, for states with a higher value of j^2-j, the potential curve is higher, particularly near the origin; states with a higher value of j will merge into the continuum for larger values of $|V|$. It is important for our study to analyze the properties of the wave function as these solutions merge into

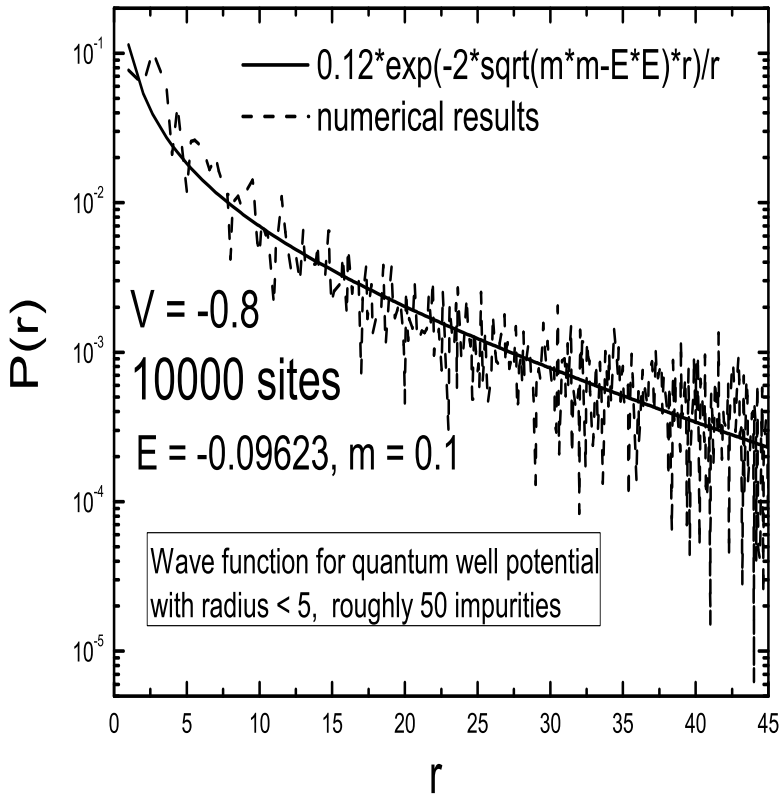

Figure 2.3: Asymptotic behavior of wave function (solid line) with energy close to the band edge for quantum well potential obtained in Dirac approximation (2.9), with an normalization constant adjusted for clarity. The exponential decay observed on the picture is in a good agreement with the results calculated in tight-binding approximation (dashed Line). The wave function becomes less localized (or more extended) as the energy approaches the top of the valence band (E=-0.1). This trend is quite different from what is known about long-range potentials. It is known that in the presence of Coulomb potential the critical wave function near the band edge is localized [11].

the continuum away from the potential wave. In fact, screening properties of the supercritical electronic liquid are controlled by the solutions' asymptotic outside the well when $E \to -m + 0$:

$$\begin{aligned} |\Psi_A|^2 &= |A(r)|^2/r \simeq \frac{C_2^2}{r}\frac{E+m}{(E-m)\sqrt{m^2-E^2}}e^{-2\sqrt{m^2-E^2}r} \\ |\Psi_B|^2 &= |B(r)|^2/r \simeq -\frac{C_2^2}{r}\frac{1}{\sqrt{m^2-E^2}}e^{-2\sqrt{m^2-E^2}r}, \end{aligned} \tag{2.9}$$

We see, that spacial distribution of electronic density is independent of the value of j. The integral of $|\Psi_B|^2$ over the plane r, ϕ diverges as $\frac{1}{\sqrt{m^2-E^2}}$. This means that the state at the moment of merging into the continuum becomes extended and is not localized in the potential well. Following the discussion of section VI in paper [11] (see also 2.4), we conclude that the merging state does not significantly alter the valence band and there will be no abrupt increase of electronic density near the impurity. Therefore, no supercritical phenomena occur in the presence of a short-range potential. This does not mean that there are no levels at the energy $E = -m$ in Dirac approximation, but states with $j = 1/2, -1/2, -3/2$, which are the lowest, are non-normalizable (or extendable) so that they do not cause critical screening. This is one the main results of my studies and we will prove this finding with computations on the lattice, as described in the subsequent sections.

The Dirac approximation for graphene gives correct predictions for electronic properties far from impurities when the coupling strength is such that the level in the gap is about to dive into the lower continuum. However, for sufficiently large coupling strength the Dirac approximation incorrectly predicts that the impurity level passes into the continuum. While we show that there is a solution in the

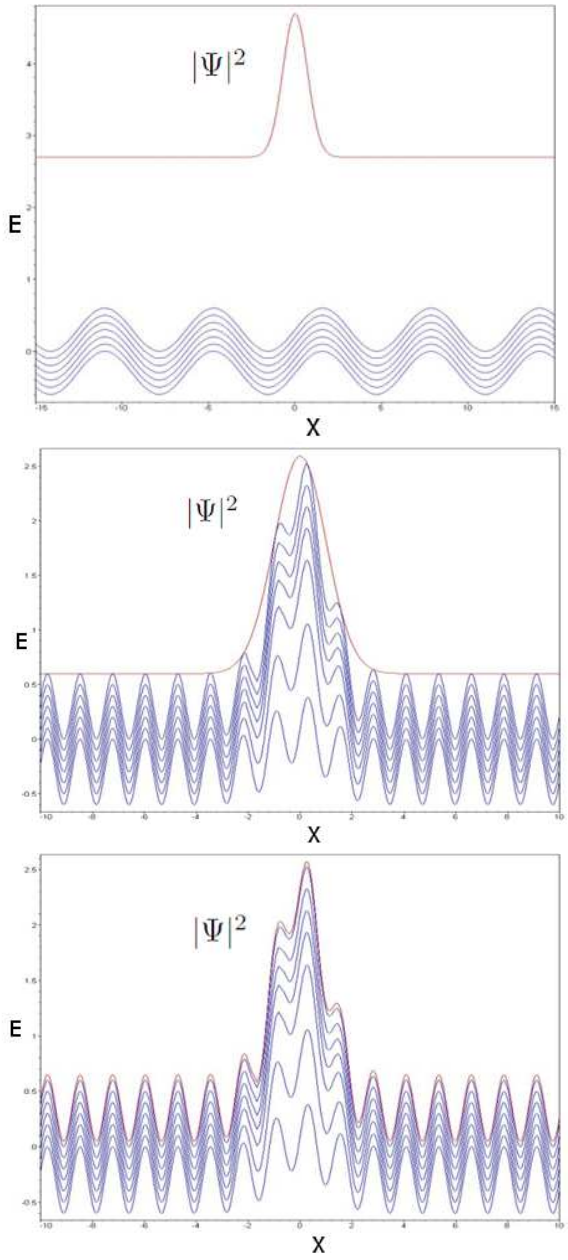

Figure 2.4: The sequence of figures illustrates midgap state merging with the lower continuum. Midgap state and states in the continuum are represented by the squares of their wave functions along some line X crossing the potential well. Top: Midgap state is far from the band edge. Middle: The midgap state just before it merges with the continuum. Probability density in the top of the valence band closely follows the shape of the merging wave function. Bottom: Even after the merging the electronic density of the continuum keeps the shape of the merged level. Thus, if the merging state is localized at the moment of diving, then the resonance consisting of quasilocalized states in the top of the valence band forms and the supercritical screening takes place.

gap for a single impurity on the lattice in a subsequent section, computations with the Dirac approximation and a delta-function potential well [22] show that the problem becomes ill-defined. If we try to find the approximate solution of the single impurity with a potential well of finite radius as we did in this section, we find that the midgap state dives into the lower continuum at the finite potential value (2.7). On contrary, in the case of the single impurity on the lattice, it is required that coupling strength is infinite. This discrepancy is due to the limitations of the Dirac approximation as it breaks down at short distances. In the following sections, we will show that requirement to have an infinite coupling strength in order to make midgap states dive also holds, if two or more impurities of the same kind are localized in the finite area on the infinite lattice.

2.3 Analytical results for one and two impurities on the lattice

2.3.1 Lattice Green function

The Hamiltonian of a free electron on the two-dimensional gapped graphene lattice, using the tight binding model is,

$$H_0 = -t \sum_{\mathbf{j},\delta} (a^\dagger_{\mathbf{j}} b_{\mathbf{j}+\delta} + b^\dagger_{\mathbf{j}+\delta} a_{\mathbf{j}}) + m \sum_{\mathbf{i}} (a^\dagger_{\mathbf{i}} a_{\mathbf{i}} - b^\dagger_{\mathbf{i}} b_{\mathbf{i}}), \tag{2.10}$$

where $a^\dagger_j$ is the creation operator of an electron on the A-atom site labeled j in the honeycomb lattice, and $b_{j+\delta}$ represents the annihilation of an electron on the neighboring B-atom site labeled $j+\delta$. Here δ denotes the three vectors that connect

an A-atom site to its three nearest neighboring B-atom sites. The parameters t and m represent the nearest neighbor hopping probability and the mass differentiating the A and B sublattices, respectively. The Hamiltonian in k-space can be written as:

$$\widehat{H}_0 = \begin{pmatrix} m & \phi_k \\ \phi_k^* & -m \end{pmatrix}, \tag{2.11}$$

where we have adopted the standard spinor notation for the A and B sublattice components of the wave function. Here, $\phi_k = -te^{-ik_x a}(1+2\cos(k_y\sqrt{3}a/2)e^{ik_x a3/2})$, where a is the distance between neighboring atoms. The eigenvalues are

$$\epsilon_{\mathbf{k},\pm} = \pm\sqrt{t^2(1+4c_y^2+4c_xc_y)+m^2}, \tag{2.12}$$

where $c_x \equiv \cos 3k_x a/2$ and $c_y \equiv \cos\sqrt{3}k_y a/2$. The Green functions in k-space can be obtained straightforwardly as

$$\mathbb{G}_0(\mathbf{k},\omega) = \begin{bmatrix} G^0_{AA}(\mathbf{k},\omega) & G^0_{AB}(\mathbf{k},\omega) \\ G^0_{BA}(\mathbf{k},\omega) & G^0_{BB}(\mathbf{k},\omega) \end{bmatrix}, \tag{2.13}$$

where ω is the energy, and each component is given by

$$\begin{aligned} G^0_{AA}(\mathbf{k},\omega) &= \frac{\omega+\mu+m}{(\omega+\mu)^2-\varepsilon_k^2} \\ G^0_{BB}(\mathbf{k},\omega) &= \frac{\omega+\mu-m}{(\omega+\mu)^2-\varepsilon_k^2} \\ G^0_{AB}(\mathbf{k},\omega) &= \frac{\phi_k^*}{(\omega+\mu)^2-\varepsilon_k^2} \\ G^0_{BA}(\mathbf{k},\omega) &= \frac{\phi_k}{(\omega+\mu)^2-\varepsilon_k^2}. \end{aligned} \tag{2.14}$$

We have added μ, the chemical potential, for completeness, and the superscript '0' serves to remind us that these Green functions are applicable to the clean lattice, i.e. without impurity scattering. The lattice Green functions in real space can be obtained by Fourier transform from the above Green's functions:

$$\mathbb{G}_0(l,j,\omega) = \begin{bmatrix} G^0_{AA}(l,j,\omega) & G^0_{AB}(l,j,\omega) \\ G^0_{BA}(l,j,\omega) & G^0_{BB}(l,j,\omega) \end{bmatrix},$$

where

$$\begin{aligned} & G^0_{AA}(l,j,i\omega_n) \\ = \; & \frac{(\omega+\mu+m)}{8\pi^2/3\sqrt{3}} \int_{-2\pi/3a}^{2\pi/3a} dk_x \int_{-4\pi/3\sqrt{3}a+|k_x|/\sqrt{3}}^{4\pi/3\sqrt{3}a-|k_x|/\sqrt{3}} dk_y \\ & \times \frac{e^{i3k_x(l_x-j_x)/2} e^{i\sqrt{3}k_y(l_y-j_y)/2}}{(\omega+\mu)^2 - m^2 - t^2(1+4c_y^2+4c_xc_y)}, \end{aligned} \tag{2.15}$$

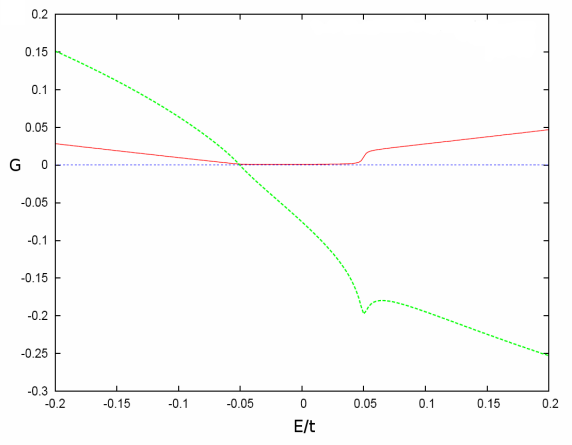

Figure 2.5: Imaginary (solid line) and real (dashed line) parts of the $G^0_{AA}(l,l,\omega)$ computed by the numerical integration of (2.15).

$$
\begin{aligned}
& G^0_{AB}(l,j,i\omega_n) \\
= \; & \frac{1}{8\pi^2/3\sqrt{3}} \int_{-2\pi/3a}^{2\pi/3a} dk_x \int_{-4\pi/3\sqrt{3}a+|k_x|/\sqrt{3}}^{4\pi/3\sqrt{3}a-|k_x|/\sqrt{3}} dk_y \\
& \times \frac{\phi_k^* e^{i3k_x(l_x-j_x)/2+ik_xa/2} e^{i\sqrt{3}k_y(l_y-j_y)/2}}{(\omega+\mu)^2 - m^2 - t^2(1+4c_y^2+4c_xc_y)}.
\end{aligned} \tag{2.16}
$$

The remaining components are readily obtained through the relations $G^0_{BB}(l,j,\omega) = G^0_{AA}(l,j,\omega,m\to -m)$ and, for the off-diagonal components,

$$
G^0_{BA}(l,j,\omega) = [G^0_{AB}(l,j,\omega)]^*. \tag{2.17}
$$

Using the traditional trick in Green functions theory , $\omega \to \omega + i\delta$, we obtain the Green functions slightly above the real axis, corresponding to the retarded Green function. For the particular case of $l = j$ (an on-site Green function), we can obtain the diagonal components analytically. From now on we set t=1, which means that all energies are measured in units of the hopping energy. The result for G^0_{AA} is (we set $\mu = 0$ for simplicity, and use the definition $E^2 = |\omega^2 - m^2|$):

(i) For $0 < E < 1, \omega^2 - m^2 < 0$,

$$
\begin{aligned}
\mathrm{Re}[G^0_{AA}(l,l,\omega)] &= -\frac{(\omega+m)}{\pi} \frac{2}{\sqrt{\left(\sqrt{E^2+1}\right)^3 \sqrt{E^2+9}}} \\
&\quad \times F\Big(\frac{\pi}{2}, \frac{1}{2}\sqrt{\frac{-(E^4+12E^2-6)}{\left(\sqrt{E^2+1}\right)^3\sqrt{E^2+9}}+2}\Big), \\
\mathrm{Im}[G^0_{AA}(l,l,\omega)] &= 0.
\end{aligned}
$$

(ii) For $0 < E < 1, \omega^2 - m^2 > 0$

$$\begin{aligned}\mathrm{Re}[G^0_{AA}(l,l,\omega)] &= -\frac{(\omega+m)}{\pi}\frac{4}{\sqrt{3-E}\left[\sqrt{(E+1)}\right]^3} \\ &\quad \times F(\frac{\pi}{2}, \sqrt{\frac{[3+E]\,(1-E)^3}{[3-E]\,(E+1)^3}}),\end{aligned}$$

$$\begin{aligned}\mathrm{Im}[G^0_{AA}(l,l,\omega)] &= -\frac{2(\omega+m)}{\pi}\frac{1}{\sqrt{3-E}\left[\sqrt{(E+1)}\right]^3} \\ &\quad \times F(\frac{\pi}{2}, \sqrt{\frac{16E}{[3-E]\,(E+1)^3}}).\end{aligned}$$

(iii) for $1 < E < 3$

$$\begin{aligned}\mathrm{Re}[G^0_{AA}(l,l,\omega)] &= \frac{(\omega+m)}{2\pi}\frac{1}{\sqrt{E}} \times F(\frac{\pi}{2}, \sqrt{\frac{(E+3)\,(E-1)^3}{16E}}), \\ \mathrm{Im}[G^0_{AA}(l,l,\omega)] &= -\frac{(\omega+m)}{2\pi}\frac{1}{\sqrt{E}}F(\frac{\pi}{2}, \sqrt{\frac{[3-E]\,(E+1)^3}{16E}}).\end{aligned}$$

(iv) for $E > 3$

$$\begin{aligned}\mathrm{Re}[G^0_{AA}(l,l,\omega)] &= \frac{2(\omega+m)}{\pi}\frac{1}{\sqrt{(E+3)\,(E-1)^3}} \\ &\quad \times F(\frac{\pi}{2}, \sqrt{\frac{16E}{(E+3)\,(E-1)^3}}), \\ \mathrm{Im}[G^0_{AA}(l,l,\omega)] &= 0.\end{aligned}$$

In these expressions we have used $F(\frac{\pi}{2}, x) \equiv \int_0^{\pi/2}(1 - x\sin^2\theta)^{-1/2}\, d\theta$, which is a complete elliptic integral of the first kind (also denoted as $K(x)$).[23]

2.3.2 Analytical formalism

We start with the equation

$$\hat{G} = (\hat{I} - \hat{G}^0\hat{V})^{-1}\hat{G}^0, \tag{2.18}$$

where $\hat{G}$ denotes a matrix where different rows (and columns) correspond to different lattice sites (an explicit example below will make this clearer, see also Ref. [24]).

As an example, we consider the specific case with two on-site impurities located at the sites labeled 0 and 1 (without loss of generality, we number the first atom on the A sublattice as 0, and we number the first atom on the B sublattice as 1; since the lattice is bi-partite, A-atoms are denoted by even numbers, and B-atoms are denoted by odd numbers). The $\hat{I} - \hat{G}_0\hat{V}$ matrix is then written explicitly as

$$\hat{I} - \hat{G}_0\hat{V} = \begin{pmatrix} 1 - VG^0_{00} & -VG^0_{01} & 0 & 0 & \dots \\ -VG^0_{10} & 1 - VG^0_{11} & 0 & 0 & \dots \\ -VG^0_{20} & -VG^0_{21} & 1 & 0 & \dots \\ -VG^0_{30} & -VG^0_{31} & 0 & 1 & \dots \\ \dots & \dots & \dots & \dots & \dots \end{pmatrix}, \tag{2.19}$$

where now the subscripts refer to the two site indices (previously written as arguments in, say, Eq. (2.15)), and V is the strength of the impurity potential at both sites. Then

$$G_{jj} = \sum_k (I - G^0V)^{-1}_{jk} G^0_{kj} = C_{kj}G^0_{kj}/\Delta, \tag{2.20}$$

where $\mathbb{C}$ is a cofactor in the matrix (2.19), and Δ is the determinant of $\hat{I} - \hat{G}^0\hat{V}$.

The factor C_{kj} is $(-1)^{k+j}$ times the determinant of the original matrix excluding the k-th row and j-th column. Eq. (2.20) can be expressed as:

$$\begin{aligned} G_{jj} &= C_{kj}G^0_{kj}/\Delta \\ &= \left[\sum_k C_{jj}G^0_{jj} + \sum_{k\leq l, k\neq j} C_{kj}G^0_{kj} + \sum_{k>l, k\neq j} C_{kj}G^0_{kj}\right]/\Delta. \end{aligned} \tag{2.21}$$

Here the number l is given by the number of sites occupied by an impurity.

For $j > l$ (away from the impurities), $\sum_{k>l,k\neq j} C_{kj}G^0_{kj} = 0$ in Eq. (2.21). In this case Eq. (2.21) becomes:

$$G_{jj} = \sum_k C_{kj}G^0_{kj}/\Delta = \left[C_{jj}G^0_{jj} + \sum_{k\leq l, k\neq j} C_{kj}G^0_{kj}\right]/\Delta. \tag{2.22}$$

The cofactor C_{jj} is equal to Δ, and therefore

$$G_{jj} = G^0_{jj} + \left[\sum_{k\leq l, k\neq j} C_{kj}G^0_{kj}\right]/\Delta. \tag{2.23}$$

Note that when $\omega = -m$, $G^0_{00}(\omega + i\delta) \sim 0$.

2.3.3 Single impurity scattering

Single impurity on the lattice is the simplest situation possible and we consider it first. We need to estimate values of G^0_{ij} to be able to compare them with each other (in what following $\omega = -m + i\epsilon$ is suggested).

$$G^0_{BB}(\mathbf{0}) = \int \frac{(-2m+i\epsilon)e^{i\mathbf{kR}}/(-2m)}{\frac{\|\epsilon_k\|^2}{2m}+i\epsilon}kdkd\phi = -\frac{1}{4m}\int \frac{(-2m+i\epsilon)e^{i\mathbf{kR}}}{\frac{\|\epsilon_k\|^2}{2m}+i\epsilon}d(k^2)d\phi, \tag{2.24}$$

where $\mathbf{R}$ is the radius-vector between two points on the lattice. We make substitution, which at least locally near K-point should work. Remembering that we need quite rough estimates for our purposes, such that we know that Gs are either infinite or finite or zero, and that is defined by the behavior near K-points:

$$\frac{\|\epsilon_k\|^2}{2m} = y,\ dy = \frac{1}{2m}\frac{d\|\epsilon_k\|^2}{d(k^2)}d(k^2) \tag{2.25}$$

Now we use Sokhatsky-Weierstrass theorem, but on the half of the real axis as $y \geqslant 0$, so we will have a half of delta-function and Lebesgue integral instead Cauchy principal value. We also move the center of coordinates to the one of the K-points ($\mathbf{K}'$) and limit the integration region by the circle of some finite radius:

$$G^0_{BB}(\mathbf{R}) = m\int \frac{e^{i\mathbf{kR}}\left[\frac{d\|\epsilon_k\|^2}{d(k^2)}\right]^{-1}}{y+i\epsilon}dyd\phi = m\int_0^{2\pi}\left\{-i\frac{\pi}{2}e^{i\mathbf{K'R}} + \int_0^{r_0}\frac{e^{i\mathbf{kR}}\left[\frac{d\|\epsilon_k\|^2}{d(k^2)}\right]^{-1}}{y}dy\right\}d\phi \tag{2.26}$$

We know that $\frac{d\|\epsilon_k\|^2}{d(k^2)} \sim 1$ as $y \to 0$, that means that second integral diverges logarithmically. The question is if this logarithmical divergency has both real and imaginary part. It appears that it has not. Indeed, $\frac{d\|\epsilon_k(\phi)\|^2}{d(k^2)} = \frac{d\|\epsilon_k(\phi+\pi)\|^2}{d(k^2)}$; $e^{ikR\cos(\phi)} = (e^{ikR\cos(\phi+\pi)})^*$, after integration over ϕ imaginary part of logarithmic

divergency cancels, hence G^0_{BB} has finite imaginary and divergent real part at $\omega = -m$

Estimation of G^0_{AB} is done in analogous way:

$$G^0_{AB}(\mathbf{R}) = -\int \frac{e^{i\mathbf{kR}}/(-2m)\epsilon^*_k}{\frac{\|\epsilon_k\|^2}{2m}+i\epsilon} k dk d\phi = \frac{1}{2}\int \frac{e^{i\mathbf{kR}}\left[\frac{d\|\epsilon_k\|^2}{d(k^2)}\right]^{-1}\epsilon^*_k}{y+i\epsilon} dy d\phi = \frac{1}{2}\int_0^{2\pi}\left\{-i\frac{\pi}{2}e^{i\mathbf{K'R}}\times 0 + \int_0^{r_0}\frac{e^{i\mathbf{kR}}\left[\frac{d\|\epsilon_k\|^2}{d(k^2)}\right]^{-1}\epsilon^*_k}{y} dy\right\} d\phi \tag{2.27}$$

As $|\epsilon_k\|^2 \sim \sqrt{y}$ if $y \to 0$ the last integral converges and it is real for the same reasons as in case of G^0_{BB}.

$$G^0_{AA}(\mathbf{0}) = \int \frac{(\omega+m)}{\omega^2 - m^2 - \epsilon_k^2} k dk d\phi \tag{2.28}$$

We need an asymptotic form of this at $\omega \to -m + 0$, using the same substitution (2.25) and defining $\omega_1 = -m + \omega$ we obtain:

$$G^0_{AA} = \frac{1}{2}\int \frac{\omega_1}{-2m\omega_1 + \omega_1^2 - \epsilon_k^2} k dk d\phi \simeq -\frac{1}{4m}\int \frac{\omega_1\left[\frac{d\|\epsilon_k\|^2}{d(k^2)}\right]^{-1}}{\omega_1 + y} dy d\phi, \tag{2.29}$$

where we neglected ω_1^2, and we obtain the leading term at $\omega_1 \to 0$:

$$K\omega_1 \ln \omega_1, \tag{2.30}$$

where $K = \frac{\pi}{2m}$. The results above will be extensively used throughout this chapter.

2.3.4 Impurity-induced inter-gap states strength

Using asymptotes obtained, let us compute the spectral weight of the inter-gap bound state near the band edge. When there is only one impurity at any A-atom site, the Hamiltonian is given by $\hat{H} = \hat{H}_0 + \hat{H}_1$, where $\hat{H}_1 = \hat{V}$. The corresponding Green functions corresponding to the two Hamiltonians are $\hat{G}_0(z) = (z - \hat{H}_0)^{-1}$ and $\hat{G}(z) = (z - \hat{H})^{-1}$. By using the T-matrix expansion, we obtain the Green function in the presence of a single impurity:

$$G_{ij} = G^0_{ij} + \frac{G^0_{i0} V G^0_{0j}}{1 - V G^0_{00}}. \tag{2.31}$$

The local density of states (LDOS) at any position on the graphene lattice is defined by the imaginary part of the Green function:

$$\rho(j, j, \omega) = -\frac{1}{\pi} \mathrm{Im} G_{jj}(\omega + i\delta), \tag{2.32}$$

and we have restored the explicit frequency dependence for clarity.

The local density of states at the impurity site is $\rho(0, 0, \omega) = -\frac{1}{\pi} \mathrm{Im} \left(\frac{G^0_{00}(\omega + i\delta)}{1 - V G^0_{00}(\omega + i\delta)} \right)$. The position of the bound state in the gap is determined by the solution of the equation $1 - V G^0_{00}(\omega + i\delta) = 0$. At the lower band edge where $\omega \to -m$, $G^0_{00}(\omega + i\delta) \sim \omega + m = 0$. Therefore, inspection of the above equation suggests that no solution exists, unless $V \to -\infty$. This observation implies that for any V the bound state will not merge into the lower continuum, i.e. no bound state energy crosses the edge at $\omega = -m$. For a single impurity on a B-atom site, the same remarks apply for a positive impurity potential, and the upper band edge plays the role previously played by the lower band edge.

To understand how the bound state approaches the continuum band edge, we use the asymptotic expansion of the complete elliptic integral of the first kind [23] to get

$$G_{00}(\omega + i\delta) \simeq \frac{K(\omega + m)\ln|\omega + m|}{1 - VK(\omega + m)\ln|\omega + m|}; \tag{2.33}$$

where $K = \frac{1}{\sqrt{3}\pi}$ By expanding the Green function near $\omega = -m$ we obtain a pole with spectral weight $a_0 = -K\omega_1^2 \ln\omega_1$, where $\omega_1 \equiv \omega + m$ is the solution of

$$1 - VK\omega_1 \ln\omega_1 = 0. \tag{2.34}$$

It is clear that as $\omega_1 \to 0$ a solution will only occur as $V \to -\infty$, and the residue corresponding to that solution approaches zero.

At the other extreme, for a very weak (negative) impurity potential, a similar expansion near $\omega \sim m$ gives a bound state energy asymptotically approaching the upper band edge (let $\omega_2 \equiv m - \omega$):

$$\omega_2 \approx \exp\frac{-1}{2mK|V|}. \tag{2.35}$$

The spectral weight approaches zero here as well, as $a_0 = 2mK\omega_2 \ln^2\omega_2$, which also goes to zero as the upper band edge is approached.

To summarize the results of this section, we showed that, as the (negative) impurity potential decreases from zero towards negative infinity, the frequency of the pole migrates from $+m$ (upper band edge) to $-m$ (lower band edge). As this occurs, the spectral weight first starts from zero, grows to some maximum, and then decreases again to zero, as the strength of the potential varies from zero to negative infinity.

2.4 Two or more impurity scattering

2.4.1 Exact solution for two impurities

We now consider the two-impurity case, with one on an A-site, $(0,0)$, and the second on a B-site $\mathbf{i}(\mathrm{i}_x,\mathrm{i}_y)$. The Hamiltonian is

$$\hat{H} = \hat{H}_0 + \hat{V} + \hat{V}_2 = \hat{H}_1 + \hat{H}_2,$$

where $\hat{H}_1 = \hat{H}_0 + \hat{V}$ as in the single impurity case. The Green functions G^0, G^1 and G correspond to $\hat{H}_0, \hat{H}_1$ and $\hat{H}$, respectively. The T-matrix for this case is

$$\hat{T} = \hat{H}_2 + \hat{H}_2\hat{G}^1\hat{H}_2 + ...$$

Therefore, the Green function becomes

$$G_{jk} = G^1_{jk} + \frac{G^1_{j\mathbf{i}} V_2 G^1_{\mathbf{i}k}}{1 - V_2 G^1_{\mathbf{i},\mathbf{i}}}.$$

In fact, for the many-impurity case, the T-matrix method can be used in a recursive way,

$$\hat{G}^n = \hat{G}^{n-1} + \hat{G}^{n-1}\hat{T}_n\hat{G}^{n-1},$$

where

$$(T_n)_{\mathbf{i},\mathbf{i}} = \frac{V_n}{1 - V_n(G^{n-1})_{\mathbf{i},\mathbf{i}}}.$$

To compute the local density of states at site $(0,0)$, we need $G_{00}(\omega)$ (for sim-

plicity we suppress the $i\delta$):

$$\begin{aligned} G_{00}(\omega) &= G^1_{00}(\omega) + \frac{G^1_{01}(\omega)V_2G^1_{10}(\omega)}{1 - V_2G^1_{11}(\omega)} \\ &= \frac{G^0_{00}(\omega)\left[1 - V_2G^0_{11}(\omega)\right] + V_2|G^0_{01}(\omega)|^2}{\left[1 - V_2G^0_{11}(\omega)\right]\left[1 - VG^0_{00}(\omega)\right] - VV_2|G^0_{01}(\omega)|^2} \\ &= \frac{F(\omega)}{(\omega - \omega_0) + i\delta}, \end{aligned} \tag{2.36}$$

where ω_0 is the energy of the pole, and $F(\omega)$ accounts for the remaining (non-singular) frequency dependence and we used (2.31) to express G^1 in terms of G^0. The actual pole position is the solution of

$$\left[1 - V_2G^0_{11}(\omega_0)\right]\left[1 - VG^0_{00}(\omega_0)\right] = VV_2|G^0_{01}(\omega_0)|^2, \tag{2.37}$$

and the spectral weight is given by $F(\omega_0)$.

Then the Green function in the case $V_2 = V$ is given by

$$G_{00}(\omega) = \frac{G^0_{00}(1 - VG^0_{11}) + V|G^0_{01}|^2}{(1 - VG^0_{00})(1 - VG^0_{11}) - V^2|G^0_{01}|^2}. \tag{2.38}$$

Keeping the leading term for G^0_{11}, we find

$$G^0_{11}(\omega) \simeq -2mK \ln \omega, \tag{2.39}$$

$$a_0 = \frac{C\omega_1}{2mK}, \tag{2.40}$$

where the quantity $C = |G^0_{01}|^2$ is finite near $\omega = -m$, and we get the result near

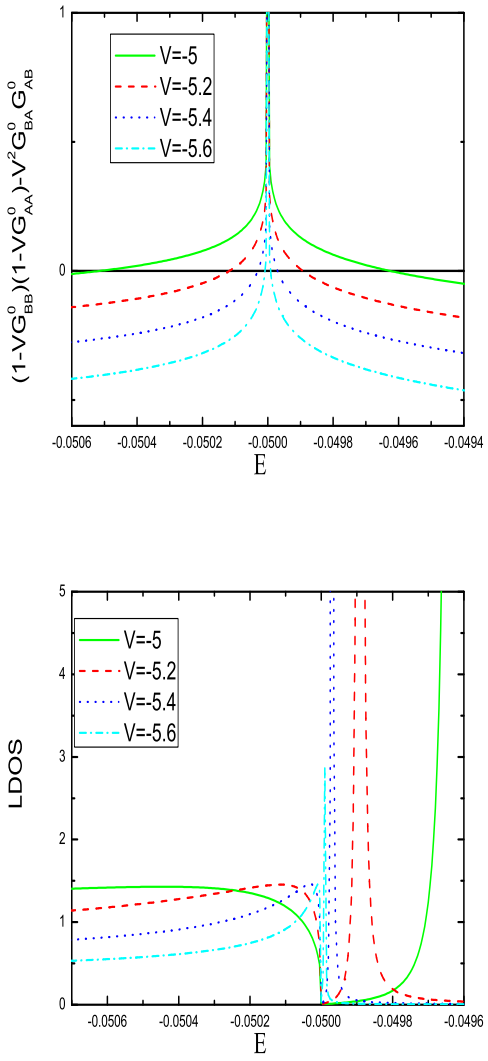

Figure 2.6: The behavior of LDOS near the valence band edge for two impurities. As the strength of the attractive impurity potential increases, the bound state inside the gap moves towards the top of the valence band, but never merges with it. The spectral weight associated with the bound state decreases to zero as the bound state approaches the band edge. This behavior is quite different from the one of a long-range impurity potential such as the Coulomb potential.

the bottom of the upper band:

$$a_0 = 2mK\omega_2 \ln^2 \omega_2, \tag{2.41}$$

The definitions of ω_1, ω_2 are the same as in the case of single impurity scattering discussed in the previous section. The conclusion is the same: as the strength of the impurity interaction increases, the pole moves towards the top of the bottom band, but never crosses it. Instead, the residue associated with the pole decreases to zero, see Fig.2.6. The key difference with the Coulomb case is that these are short range impurities, and this leads to qualitatively different behavior.

2.4.2 Long-range asymptotes of the Green functions for a large number of impurities

In this subsection we generalize to some extent the results obtained in the previous sections. We find in the thermodynamic limit the long-range asymptotic behavior of the Green function in the case of multiple impurities located inside a finite area of the graphene sheet. We also discuss the quantity of the on-site potential required for midgap energy states to join the valence band. As a particular case this discussion includes the circular well, discussed in the Dirac approximation, at the beginning of the chapter in Section II. Knowing these Green functions' asymptotes, we show that the spectral weight of the state near the band edge (on the verge of entering into the lower continuum) is zero and the screening charge is not significantly reshaped by this state.[11]

We rewrite Eq. (2.23):

$$G_{\mathbf{RR}} = G^0_{\mathbf{RR}} + \left[\sum_{r\leq a} C_{\mathbf{rR}} G^0_{\mathbf{rR}}\right]/\Delta. \tag{2.42}$$

Here we introduced the following notation: R is the distance from the center of the area in which the impurities are confined; we will call this area the "potential well"; $\mathbf{R}$ corresponds to the site index outside the well; a is the radius of the well; r and r' are the distances inside the circle of radius a, and $\mathbf{r}$ is the index of the site inside the well.

The second term in Eq. (2.42) represents the change induced by the impurity and is responsible for the spectral weight of the bound state. Assuming $R \gg a$, the following conclusions can be made about the second term. Δ does not depend on R, but $C_{\mathbf{rR}}$ depends on R, and $C_{\mathbf{rR}} \sim G^0_{\mathbf{rR}}$, as the determinant $C_{\mathbf{rR}}$ contains only one row with $G^0_{\mathbf{rR}}$.

Considering the sum over $\mathbf{r}$ in $\sum_{r\leq a} C_{\mathbf{rR}} G^0_{\mathbf{rR}}$ we see that the r dependency comes only from the phase $\overrightarrow{k}\cdot(\overrightarrow{R}-\overrightarrow{r})$ in the exponent of the integrands (2.15, 2.16). At the energies near the band edge $\omega \to -m$, the part $\overrightarrow{k}\cdot\overrightarrow{r}$ can be neglected, as the small k's produce most of the integral value and $\overrightarrow{k}\cdot\overrightarrow{r}$ does not vary significantly near the Dirac point. Therefore,

$$\sum_{r\leq a} C_{\mathbf{rR}} G^0_{\mathbf{rR}} \sim (G^0_{\mathbf{0R}})^2. \tag{2.43}$$

The spatial dependance of the second term in $G_{\mathbf{RR}}$ is determined by the $(G^0_{\mathbf{0R}})^2$, where $\mathbf{0}$ denotes some (arbitrary chosen) site in the impurity-occupied area. To determine the asymptotic behavior of $G^0_{\mathbf{0R}}$, we use the method of stationary phase

(see problem 5.2 in [25]), and get

$$G^0_{\mathbf{0R}}(\omega \to -m) \sim \frac{\exp(-R\sqrt{\delta E})}{(\delta E)^{1/4}\sqrt{R}}, \tag{2.44}$$

where $\delta E = m^2 - \omega^2$. Thus $G_{\mathbf{RR}} \sim \frac{\exp(-2R\sqrt{\delta E})}{(\delta E)^{1/2}R}$, in qualitative agreement with the asymptotic behavior predicted by the Dirac equation (2.9). As we can see from the standard definition of the Green function [25]:

$$G_{\mathbf{RR'}}(\omega) = \sum_n \frac{\psi_n(\mathbf{R})\psi_n(\mathbf{R'})^*}{\omega - \omega_n} + \int dc \frac{\psi_c(\mathbf{R})\psi_c(\mathbf{R'})^*}{\omega - \omega_c} \tag{2.45}$$

when $\omega \to \omega_n$ the r-dependency of $G_{\mathbf{RR}}(\omega)$ coincides with $\psi_n(\mathbf{R})\psi_n(\mathbf{R})^*$. Therefore, we can judge if the state that is potentially crossing the band edge into the continuum is normalizable. In our case as $\delta E \to 0$ the sum of $G_{\mathbf{RR}}$ over $\mathbf{R}$ in the plane diverges, and so does the sum $\psi_n(\mathbf{R})\psi_n(\mathbf{R})^*$ in the infinite lattice for any finite normalizing factor. Hence the state merging into the continuum can be called non-normalizable or extended and as such has zero spectral weight (in the thermodynamic limit). This confirms our conclusion that there is no such phenomenon like supercritical screening in the case of a localized potential (as opposed to a Coulomb potential) in graphene.

Another question to address is whether the energy of the state penetrates into the continuum at reasonable values of the on-site potential or not. To answer this question, we rearrange terms in the matrix (2.19) in the following way (this example includes two impurities on sublattice A and two impurities on sublattice

B, all with strength V):

$$\hat{I} - \hat{G}_0\hat{V} = \begin{pmatrix} 1 - VG^0_{A_1A_1} & -VG^0_{A_1A_2} & -VG^0_{A_1B_1} & -VG^0_{A_1B_2} & \\ -VG^0_{A_2A_1} & 1 - VG^0_{A_2A_2} & -VG^0_{A_2B_1} & -VG^0_{A_2B_2} & \\ -VG^0_{B_1A_1} & -VG^0_{B_1A_2} & 1 - VG^0_{B_1B_1} & -VG^0_{B_1B_2} & \\ -VG^0_{B_2A_1} & -VG^0_{B_1A_1} & -VG^0_{B_2B_1} & 1 - VG^0_{B_2B_2} & \\ .. & .. & .. & .. & .. \end{pmatrix} \tag{2.46}$$

A and B here correspond to indices on the A and B sublattice, respectively. We ignore all other terms of the matrix $(\hat{I} - \hat{G}_0\hat{V})$ because they do not influence the determinant, whose roots define the allowed energies. To estimate the value of the required potential V when the root of the secular equation $\omega_1 \to 0$, we assume that the value of potential V is finite (negative). We will show that if this is true then there is no solution for this secular equation in the limit $\omega_1 \to 0$. We use the formula:

$$\begin{pmatrix} W & X \\ Y & Z \end{pmatrix} = det(W)det(Z - YW^{-1}X). \tag{2.47}$$

With reference to Eq. (2.46), the AA elements correspond to the matrix W, BB to the matrix Z, and AB and BA to the X and Y matrices, respectively. Therefore, we can factorize our secular equation:

$$\Delta = det(W)det(Z - YW^{-1}X) = 0. \tag{2.48}$$

Let us check if there are any roots of the equation in the factor $det(W)$. It is easy to see that there are no roots because $det(W) \to 1$ when $G^0_{AA} \to 0$. In the

second cofactor the Z-term is dominating, as $G^0_{BB} \sim \ln(\omega_1)$, $det(Z - YW^{-1}X) \sim det(\{\ln(\omega_1)\})$, where $\{\ln(\omega_1)\}$ denotes the matrix of the entries with the leading term of the order of $ln(\omega_1)$. Equation $det(\{\ln(\omega_1)\}) = 0$ can be expanded as

$$det(\{\ln(\omega_1)\}) \sim O_N(1)\ln(\omega_1)^N + \\ + O_{N-1}(1)\ln(\omega_1)^{N-1} + O_{N-2}(1)\ln(\omega_1)^{N-2} + .., \quad (2.49)$$

here $O_i(x)$ denotes terms of the order of x, N is a number of impurities on B-sites. Therefore, all $O_i(1) = 0$ if $det(\{\ln(\omega_1)\}) = 0$. This scenario is highly improbable in case of multiple impurities because $O_i(1)$ are constants and are equal to the determinants of matrices consisting of coefficients near the $\ln(\omega_1)$ leading term. Each of $O_i(1)$ should be equal to zero simultaneously, as each consecutive term in (2.49) is lesser by the order of the magnitude than the previous one at $\omega_1 \to 0$. We conclude that the bound state energy does not penetrate into the valence band at a non-infinite value of the potential.

On the other hand, if the potential diverges as $\omega_1 \to 0$, a solution to the secular equation can exist. It is easy to see, for example, that in the dilute case, when impurities sit far from each other, ω_1 is the same as in the case of a single impurity on an A site, which has been considered in the previous sections.

Another question to address is whether the energy of the state penetrates into the continuum at finite values of the on-site potential or at infinite ones. As we have seen in Section II, Dirac approximation predicts diving at the finite value of V. Opposite to that, analytical results for single and two impurities on the lattice predict infinite value of the on-site potential. Therefore, one might expect that on-site potentials required for the level to dive in the tight-binding model with

multiple impurities might be significantly different from those computed within Dirac approximation. Analytical computations with many impurities involved are cumbersome, henceforth we use two numerical methods to tackle the problem. This should ensure a credibility of the results. We apply Lanczos algorithm to find energy states inside the gap and see how they move with the increase of the absolute value of the on-site potential V[2]. Another method is to use the equation [24]:

$$det(\hat{I} - \hat{G_E^0}\hat{V}) = 0. \tag{2.50}$$

Numerical procedure designed to solve the latter equation for E uses pre-tabulated values of G_E^0. Simulations are performed in case of six impurities sitting in the nodes of a hexagon and in the case of twelve impurities, where we placed six impurities in the nodes of the hexagon and another six at the next closest sites. Our results show that at finite values of V no levels descending through the gap penetrate into the valence band. Result for the well containing twelve sites are presented on the Fig.2.7.

In this subsection we make two important points about the effects induced by multiple impurities. First, we found that the lower continuum in graphene is not perturbed by the diving midgap state, which is opposite to the case of supercritical impurities with a Coulomb potential. Second, we conclude that diving of this state can only happen at very large values of the short-range potential, which can be seen from Fig.2.7.

[2]We perform computations keeping numbers of nodes in A and B sublattices equal. In the case when those numbers are not equal picture can be different, possibly due to the influence of "zero modes", localized states induced by the sublattices imbalance.

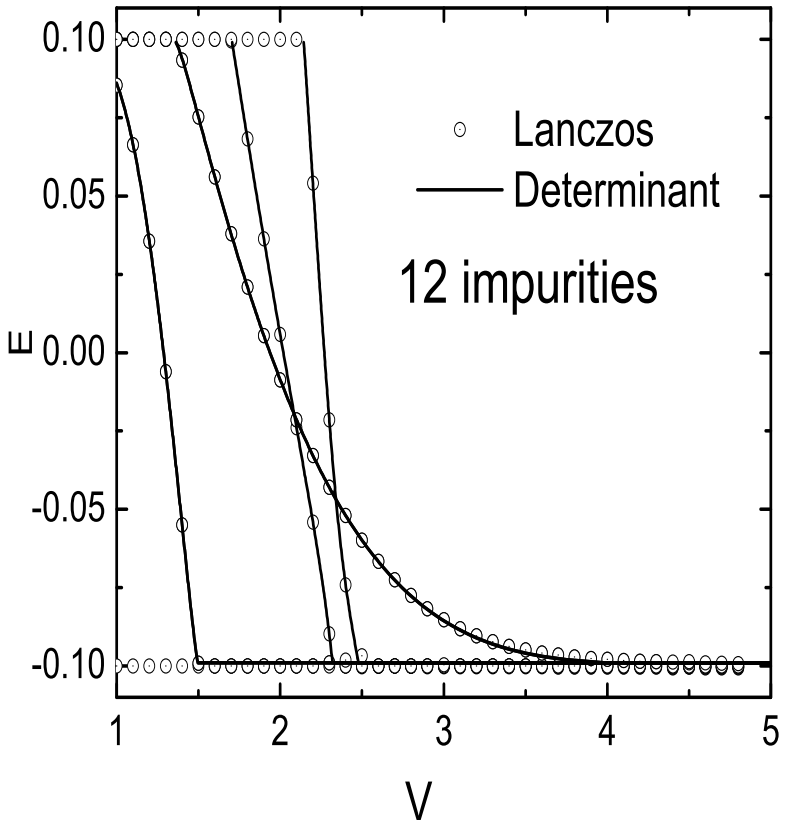

Figure 2.7: The graphs on this picture show the results of the numerical diagonalization of the Hamiltonian with Lanczos algorithm (solid lines) and matched with results from determinant method (2.50). The lattice of the 4000 atoms contains 12 impurities. Curves on the graph show the energy levels separating from the conductance band ($E = 0.1$) and descending to the valence band ($E = -0.1$ in the units of t) while $-V$ increases. Both methods confirm that midgap states do not dive into the valence band, opposite to the predictions of the long wave (Dirac) approximation.

2.5 Discussion

Let us try to match our results with common intuition developed in physics of shallow states in semiconductors. In particular, it is not only a feature peculiar to gapped graphene that properties of the states near the band edge are strongly dependent on the long range "tail" of the impurity potential.[26] In general, the effective mass approach (mostly determined by long-range properties of a system) is in good agreement with exact numerical methods for the energies near the band edge. It is exactly near the band edge where the Coulomb tail becomes important while it is negligible in computations related to deep levels.[27] As it was illustrated in [11], in the continuum limit a potential barrier emerges in the effective potential at large distances, due to the squaring of the Coulomb potential. Because of the two sublattices, a similar 'squaring' occurs when the problem is solved on a lattice, and lattice Green functions are utilized.[28]. Long wave approximation provided results which were in qualitative agreement with lattice computations in [11].

On the other hand, though the Dirac approximation is useful to describe phenomena at long distances (2.3), providing correct long wave asymptotic for the wave functions of shallow levels, it has its limitations for the short-range potentials. We showed that the Dirac approximation gives incorrect predictions about the strength of on-site potential at which diving takes place.

Conclusion

I outline the main results and conclusions presented in this thesis and discuss the novelty of results.

There are a plenty of publications discussing scattering on various impurities and potentials. In the article [18] authors discussed gapless graphene and perform computations using the Dirac approximation. They considered short-range scattering in order to estimate the conductivity at low impurities concentrations. In [20] researchers suggested and showed that the mid-gap states (induced by vacancies) at the Dirac point are the source of the enhanced scattering. This group used only Dirac approximation, however we discussed that, more reliable results should be obtained within the tight-binding approximation, which takes into account the full proper band structure for the gapped graphene. The author of [21] used the Dirac approximation to describe the physical properties of graphene with massive fermions. In this article the author mostly pays attention to the Coulomb potential, contrary to our set-up where we use short-range impurities in gapped case. In [19] the massless case is discussed and Green functions on the graphene lattice are addressed in the thermodynamic limit. Authors of papers [29] discussed the Coulomb potential in gapless graphene using the Dirac approximation.

In the present work we considered gapped graphene in both the Dirac approx-

imation and in the framework of tight-binding model. Our group modeled several various short-range-potentials on graphene lattice. This physical situation has never been investigated before in tight-binding approximation, and as our results reveal, Dirac formalism gives wrong predictions. It fails in case of short-range potentials.

One of the main results of our investigations of bound states in gapped graphene with localized impurities is the claim that the bound state's energy asymptotically approaches $-m$ (the lower continuum edge) as the impurity potential V tends to the negative infinity. We take the impurity potential in the form of a spherical well $V\theta(a-r)$. In the Dirac approximation we shown that there are energy levels merging lower continuum at the finite potential. In realistic lattice computations we found that the bound state's energy never crosses the lower continuum edge. Since the long-wave Dirac approximation and lattice approaches give different results, we performed detailed investigation of these discrepancies.

The existence of the solutions for Dirac equation with circular potential well was already known in the literature [21]. Our aim was to investigate their physical properties. The solution on the verge of merging with lower continuum is not normalizable which resembles the situation in three dimensions. The solution in 3D joins the continuum at the finite potential too, but this does not render the situation as critical. The solution should be localized or normalizable at the moment when it dives into the lower continuum, which does not happen in that case. In Akhiezer and Berestetsky's book [36], where the solution for a spherical well is described, the critical field corresponds to the coupling strength at which the $1s$ state dives into the continuum and positron-electron pairs are emitted. This state is delocalized [17], and thus does not introduce the supercritical screening

after $1s$ state merges with the continuum. As mentioned in the first chapter, under the supercritical screening we understand the abrupt increase of electronic density around the impurity after the state of the discrete spectrum joins the continuum and the merging state must be localized. According to this description, the field in which the lowest bound state joins the continuum is not a critical field. The similar situation is described in the thesis in 2D: state "dives" into the continuum at the finite negative potential, but there is no criticality as the merging state is delocalized.

Our analysis on the lattice shows that diving states' probability density is non-normalizable as well, but diving happens only at nonphysical, infinite negative potentials. The numerical computations were performed for only several impurity configurations and, due to the limitations imposed by computers available, do not cover potential wells with number of impurities higher than 20. Thus, the case of potential wells with the bigger radii is out of the scope of this work and we do not know the potential value midgap state to join the lower continuum. One statement holds, though, even in this "big radius" case, as it was proved analytically: there is no critical screening as well.

The difference between the results obtained on the lattice and those derived using the Dirac approximation is a consequence of the limited applicability of the Dirac equation. The potential is of the order of m, or the width of the gap, while the Dirac approximation only works at low energies. In other words, in the problems with short-range potentials even at the energies close to the top of valence band one needs to take into account the exact dispersion law for quasi-particles. This is a quite unusual result, as the effective mass approximation or, as it called in graphene physics, Dirac approximation is derived by expanding

the Hamiltonian near the Dirac point. We suggest that the explanation to this is that for the Dirac formalism to be applicable the potential should not change abruptly on the lengths comparable to the inter-atomic distance. This is one of the assumptions made before one starts to derive effective-mass equations and in the physical situations with short-range potentials on a lattice this assumption is not fulfilled.

The absence of critical screening in gapped graphene may have important implications for technology. Contrary to the case with Coulomb impurities where the critical screening takes place, the areas with short-range potential do not induce significant concentration of electronic density around them. The induced charge is spread around the much larger area. Hence, the scattering of the propagating electrons is much lower than in Coulomb case and, hence, the conductivity is not affected as much as in the presence of long-range potentials.

Bibliography

[1] Novoselov, K.S., A. K. Geim, S. V. Morozov, D. Jiang, Y. Zhang, S. V. Dubonos, I. V. Grigorieva, and A. A. Firsov, Electric Field Effect in Atomically Thin Carbon Films, Science **306**, 666 (2004)

[2] P. R. Wallace, The Band Theory of Graphite, Phys. Rev. **71**, 622 (1947).

[3] P. Sutter, Epitaxial graphene: How silicon leaves the scene, Nature Materials **8**, 171 (2009).

[4] H.-P. Boehm, R. Setton, E. Stumpp, Pure & Appl. Chem., **66**, 1893 (1994).

[5] D. Haberer, D. V. Vyalikh et al., Nano Lett., **10**, 3360 (2010).

[6] K. Novoselov, Nature Materials **6**, 720 (2007).

[7] M. I. Katsnelson, Materials Today, **10**, 20 (2007).

[8] A. Young, P.Kim, Nature Physics **5**, 222 (2009).

[9] J-H. Chen, W. G. Cullen, C. Jang, M. S. Fuhrer, E. D. Williams, Phys. Rev. Letters, **102**, 236805 (2009)

[10] R. R. Nair et al, Nano Letters. Article ASAP, DOI: 10.1021/nl100996u (2010).

[11] V. M. Pereira, V. N. Kotov, and A. H. Castro-Neto, Physical Review B, **78**, 085101 (2008).

[12] S. Adama, E.H. Hwanga, E. Rossia and S. Das Sarma, Solid State Communications **149**, 1072 (2009).

[13] A. Altland, B. Simons, Condensed matter field theory, Cambridge (2009).

[14] N. Ashcroft, N. Mermin, Solid State Physics, Holt, Rinehart and Winston (1976).

[15] N. M. R. Peres, F. Guinea, A. H. Castro Neto, Annals of Physics **321**, 1559 (2006).

[16] S. Y. Zhou, G. -H. Gweon, A. V. Fedorov, P. N. First, W. A. De Heer, D. -H. Lee, F. Guinea, A. H. Castro Neto and A. Lanzara, Nature Mater. **6**, 770 (2007).

[17] Ya B Zeldovich, V S Popov, Sov. Phys. Usp. **14** 673 (1972).

[18] M. I. Katsnelson and K. S. Novoselov, Solid State Commun. **143**, 3 (2007)

[19] T. O. Wehling et al, Phys. Rev. B **75**, 125425 (2007)

[20] T. Stauber et al, Phys. Rev. B **76**, 205423 (2007).

[21] D. S. Novikov, Phys. Rev. B **76**, 245435 (2007).

[22] F. A. B. Coutinho and Y. Nogami, Phys. Rev. A **42**, 5716 (1990).

[23] M. Abramowitz and I.A. Stegun, Handbook of Mathematical Functions (Dover, New York (1972).

[24] J. Callaway, A.J.Hughes, Phys. Rev. **156**, 860 (1967).

[25] Economou E.N., Green Functions in Quantum Physics, http://www.springerlink.com/content/j75035r1618442q2.

[26] S. Pantelides, Rev. Mod. Phys. **50**, 797 (1978).

[27] C. Rodriguez, S. Brand, M. Jaros, J. Phys. C: Solid St. Phys., **13**, L333 (1980).

[28] T. Morita, T. Horiguchi, J. Math. Phys **13**, 8 (1972).

[29] A. V. Shytov, M. I. Katsnelson, and L. S. Levitov, Phys. Rev. Lett. **99**, 236801 (2007).

[30] Ivan S. Terekhov, Alexander I. Milstein, Valeri N. Kotov, and Oleg P. Sushkov, Phys. Rev. Lett. **100**, 076803 (2008).

[31] Rudro R. Biswas, Subir Sachdev, and Dam T. Son, Phys. Rev. B **76**, 205122 (2007).

[32] P. K. Pyatkovskiy, arXiv:0808.931v1 (2008).

[33] Antonio H. Castro Neto, Les Houches Notes on Graphene, arXiv:1004.3682v1 (2010).

[34] B.S. Kandemira, A. Mogulkoc Eur. Phys. J. B **74**, 535 (2010).

[35] Yu. Lozovik, S. Merkulova, A Sokolik, Uspehi Fizicheskih Nauk, **178**, 7 (2008) (In Russian)

[36] A. I Akhiezer V. B Berestetsky, Quantum Electrodynamics, U.S. Atomic Energy Commission (1953).